Sex-dimorphic neuroprotective effect of CD163 in an α-synuclein mouse model of Parkinson's disease

Sara A. Ferreira[1,2], Conghui Li[4], Ida H. Klæstrup[1,2], Rikke K. Rasmussen[1], Asger Kirkegaard[1,2], Gitte U. Toft[1,2], Cristine Betzer[1,2], Pia Svendsen[1,3], Poul H. Jensen[1,2], Yonglun Luo[1,2,4], Anders Etzerodt[1], Søren K. Moestrup[1,3] and Marina Romero-Ramos[1,2]

1. Department of Biomedicine, Aarhus University, Denmark

2. Danish Research Institute of Translational Neuroscience – DANDRITE, Aarhus University, Denmark

3. Department of Cancer and Inflammation Research, Syddansk Universitet, Odense, Denmark

4. Lars Bolund Institute of Regenerative Medicine, Qingdao-Europe Advanced Institute for Life Sciences, BGI-Qingdao, BGI-Shenzhen, Shenzhen 518083, China

 # Corresponding author: Marina Romero-Ramos, Dept. of Biomedicine, Aarhus University, Hoegh-Guldbergsgade 10, DK-8000C Aarhus, Denmark. Phone: +4587167854. E-mail: mrr@biomed.au.dk

Keywords: Alpha-synuclein, microglia, macrophages, neurodegeneration, CD163KO

ABSTRACT

The aggregation of alpha-synuclein (α-syn) and immune activation are both pathological events related to the neurodegenerative process in Parkinson's disease (PD). The PD-associated immune response involves both brain and peripheral immune cells, although little is known about the immune proteins relevant for such response. CD163 is a scavenger receptor specifically expressed in the monocytic lineage, but normally not in microglia. Therefore, the presence of CD163 positive cells into the brain in PD rodent models and in PD patients suggest a monocytic infiltration or otherwise ectopic CD163 expression. In addition, changes in CD163 expression profiles observed in PD patients might indicate a role for CD163-expressing cells in the disease. To elucidate the relevance of the CD163 receptor in the α-syn-induced immune events in PD and associated degeneration we injected murine α-syn pre-formed fibrils (PFF), or monomeric α-syn into the striatum of CD163 knockout (KO) mice and wild-type (WT) littermates. Injection of α-syn PFF in CD163KO females led to impaired early immune responses as revealed by the lack of ability to upregulate MHCII, CD68, GFAP, and promote CD4 and CD8 T cell infiltration after α-syn PFF injection. An early and long-lasting sensorimotor impairment was observed in α-syn PFF CD163KO males but not in the females. Transcriptomic analysis revealed that CD163 deletion induced phenotypic changes of macrophages and microglia in the brain that potentially impact the motor behavior and neuronal health induced by α-syn in a sex-dependent manner. After 6 months, CD163KO females showed an exacerbated immune response and α-syn pathology associated with autophagic defects, which ultimately led to increased dopaminergic neurodegeneration. Overall, our results support a novel sex-dimorphic neuroprotective role for CD163 in the α-syn-induced neuropathology and immune response.

INTRODUCTION

Parkinson's disease (PD) is prototypically defined as a neurodegenerative disorder with two key neuropathological features: loss of dopaminergic neurons in the Substantia Nigra (SN) and the presence of intraneuronal alpha-synuclein (α-syn) pathological aggregates in Lewy bodies (LBs) throughout the nervous system [60]. Evidence suggest that misfolded α-syn can behave as a prion-like protein, capable of self-propagating and pathologically spread progressively throughout the nervous system via cell-to-cell transmission [75]. Indeed, *in vivo* striatal injection of human or murine α-syn preformed fibrils (PFF) in the rodent brain led to the pathological aggregation of α-syn in anatomically interconnected regions, and dopaminergic degeneration [45, 74]. These findings have resulted in the establishment of novel PD models that are potentially useful to investigate the molecular and cellular processes associated with α-syn aggregation in the brain. Among these, the immune response has been suggested to parallel, or even precede, neurodegeneration in PD, influencing neuronal health. Microgliosis, together with a marked pro-inflammatory profile, have been shown in *postmortem* PD brains [12, 49] and in α-syn-based rodent and non-human primate models [4, 64, 80]. However, the PD immune response involves not only brain-resident glial populations (microglia and astrocytes), but also entails peripheral innate (monocytes/macrophages, dendritic cells) and adaptive immune cells (T and B lymphocytes) [27]. During neurodegeneration, peripheral monocytes/macrophages are modified and can infiltrate the central nervous system (CNS) to partake in α-syn clearance and/or promote inflammation [70].

The monocytic-specific scavenger receptor CD163 is considered a marker for alternatively activated macrophages with absent expression in homeostatic microglia. CD163 expression increases upon anti-inflammatory cytokine IL-10 or glucocorticoid exposure [6], but also under certain inflammatory conditions putatively as a protective mechanism [37]. CD163 uptakes the hemoglobin/haptoglobin complexes for degradation in lysosomes. The heme part is converted by the heme-oxygenase 1, leading to metabolites with reported immunomodulatory functions [61]. However, CD163's specific role in the immune system is still undefined, although studies of CD163 knock out (CD163KO) mice point towards an overall anti-inflammatory function [68]. Increased numbers of CD163+ cells have been found in PD and Alzheimer's disease (AD) *postmortem* brains [57], in the brain of the 6-OHDA [73], and the α-

syn-PFF based models of PD [26]. CD163 expression is lost during microglia development, hence absent in adult microglia, as revealed by several single-cell RNA sequencing studies [5, 29, 31]. Thus, its expression in the brain seems associated with infiltration or otherwise ectopic upregulation of the protein. We have previously shown that soluble CD163 (sCD163), produced by shedding upon monocyte/macrophage pro-inflammatory activation, is increased in the CSF of late-stage PD patients; suggesting infiltration and activation of the CD163+ population in brain. Moreover, sCD163 in the CSF correlated to α-syn and Tau levels, as well as cognitive decline in these PD patients, revealing a role for CD163 monocytes in the disease. Notably, in serum, sCD163 levels were increased only in female but not male patients, indicating a sex-dimorphic CD163 monocytic behavior [53]. We have recently shown that the percentage of CD163 cells in the blood was associated with lower inflammation in the brain and better putaminal dopaminergic neurotransmission in REM sleep behavior disorder patients, suggesting a protective function for the CD163 cells in prodromal stages of PD [18]. Moreover, we have recently reported increased number of CD163 cells in the blood of PD patients, as well as increased cellular expression of the protein per cell [34]. We speculate that the observed increase in CD163 expression is a part of a neuroprotective compensatory mechanism.

Altogether, the data so far support a significant role for the CD163 cells in PD, however, it is yet unclear the significance of the receptor in the inflammatory process related to the disease and its consequences for the neuronal fate. To investigate this, we analyzed α-syn neurotoxicity, pathological spreading, and immune alterations in CD163KO mice by injecting α-syn PFF into the striatum of these animals vs. wild type (WT). Additionally, we performed SMARTseq2 on microglia and macrophage populations in the brain to further assess the transcriptomic and phenotypic alterations in these immune populations upon CD163 deletion. We now hypothesize that CD163 deficiency leads to macrophage impaired/pro-inflammatory phenotypes and subsequent modulation of microglia responses to α-syn PFF in a possible sex-dependent manner.

Materials and Methods:

Experimental Design

Adult male and female CD163KO ($CD163^{tm1.1(KOMP)Vlcg}$) mice and WT (C57BL/6N) littermates (n=156 total (n=83 males (43 WT + 40 CD163KO); n=73 females (39 WT+ 34 CD163KO))

were used in this study [17]. Mice weighted 20-25g (12 weeks old) at the time of the surgery and were housed maximum 4-6 per cage, with *ad libitum* access to food and water, in a climate-controlled facility under 12h/12h night/daylight cycle. All animal experiments were approved and performed under humane conditions in accordance with the ethical guidelines established by the Danish Animal Inspectorate and following EU legislation.

To generate a PD model, murine α-syn PFF were used due to their higher seeding efficiency in mice compared to human α-syn PFF [22, 44]. In parallel, mouse monomeric α-syn (MONO) was used as a control based on its reported lack of seeding capacity *in vitro* [79] and *in vivo* [45]. Mice received unilateral intrastriatal injection of α-syn MONO or α-syn PFF and were killed 1 and 6 months post-surgery. (**Suppl. Fig. 1**). The 1-month group included: α-syn MONO (Males WT n=7 & CD163KO n =8; Females WT n=6 & CD163KO n=6), and α-syn PFF (Males WT n=9 &CD163KO n =7; Females WT n=6 &CD163KO n=6). While the 6-months group consists of: α-syn MONO (Males WT n =8 & CD163KO n =9; Females WT n=8 &CD163KO n=8), and in the α-syn PFF (Males WT n=9 & CD163KO n=10, Females WT n=9, & CD163KO n=8). Motor behavior was assessed on the week before each end-point using the Challenging Beam Test and the Cylinder test. Mice were euthanized, perfused and brains processed for immunohistochemical staining.

For whole population RNA sequencing, a third and fourth group of mice (batch 1 and batch 2) received bilateral intrastriatal injection of α-syn MONO (Males WT n=7 & CD163KO n =4*; Females WT n=7 &CD163KO n=5), and α-syn PFF (Males WT n=7, & CD163KO n =5; Females WT n=7 & CD163KO n=5). Triplicates were used for sequencing. Mice were killed 2 months post-surgery, their brains dissected and the immune cells (microglia & macrophages) isolated and FACS sorted for RNA purification and subsequent SMART-seq2 sequencing. *CD163KO-MONO males were excluded from the analysis due to inconsistencies in the technical replicates. For the *in vitro* experiment, bone-marrow derived macrophages (BMDM) were isolated from CD163KO and WT C57BL/6N male and female mice, aged 6-12 weeks (n=5 per group).

Protein purification and aggregation of mouse α-synuclein

Murine α-syn was recombinantly expressed in E. coli BL21 DE3 bacteria using the pRK172 plasmid encoding for mouse α-syn (kind gift from Prof. Virginia Lee (University of

Pennsylvania)). The bacteria was pelleted by centrifugation and resuspended in buffer (50 mM Tris, 1 mM EDTA, 0.1 mM DTE, 0.1mM PMSF, pH 7.0). The suspension was lyzed by sonication in a Branson Sonifier (Output control 7; dutycycle 50), and centrifuged at 20,000 *x g* for 30 minutes at 4°C. The supernatant was boiled for 5 min and centrifuged at 48.000 *x g* for 30 min at 4° C. Preceding ion exchange purification, the supernatant was dialyzed in 20 mM Tris pH 6.5, and filtered through a 45µm filter. Murine α-syn was purified on POROS HQ 50 ion exchange chromatography with a continuous gradient of 0% - 100% 2 M NaCl in 20 mM Tris pH 6.5. The fractions with murine α-syn were isolated and further purified by reverse phase chromatography (C18) in order to remove nucleotides, and lipids bound to α-syn. This step also removes endotoxins (lipoglycans) from the sample (<0.5 EU/mg, confirmed using the Pierce™ Chromogenic Endotoxin Quant Kit, ThermoScientific™). The pure protein was dialyzed in 20 mM ammonium bicarbonate, lyophilized, and stored at -20°C. In order to produce sterile PFF, mouse α-syn was solubilized in PBS (7.2 mM Na_2HPO_4, 2.8 mM NaH_2PO_4, 140 mM NaCl, pH 7.4) to a final concentration of 7 mg/mL, and further sterile filtered through a 0.22 µm sterile filter in a LAF bench. The solution was allowed to aggregate at 37°C, 1000 RPM for 10 days. The insoluble α-syn PFF were isolated from unbound α-syn MONO by 20,000 *x g* centrifugation for 30 min at 20° C and further resuspended in fresh sterile PBS. Protein concentration was determined by Bicinchoninic acid protein concentration assay (Pierce).

Recombinant α-syn fibrils sonication and stereotaxic surgery

On the day of surgery, α-syn PFF were sonicated for 40 minutes (70ms off/30ms on, 30% output power, Branson 250 sonifier), and their hydrodynamic average length was determined prior and post-surgery by Dynamic Light Scattering (DLS) (Wyatt DynaPro NanoStar), at 25°C. Fibrils were of average =33.87nm (range: 25.90-41.10nm), thus within the optimal size range of 29-49nm previously reported [1], and remained so during the surgery day (not shown). Mice were anesthetized (Medetomidine hydrochloride (1mg/ml), Midazolam (5mg/ml) and Fentanyl (0,05mg/ml) in 0.9% NaCl for a final i/p. dose of 20ml/kg) and placed in a stereotaxic apparatus (Stoeling). α-syn PFF or α-syn MONO (2µl of 5 µg/µl, in sterile PBS) were unilaterally (or bilaterally for RNA analysis) injected into the striatum: AP +0.7/+0.9mm (females and males respectively), ML +/- 2.0mm (from bregma), and DV -3.0mm (from dura) [21]. A s.c. antagonist solution (Flumazenil (0.1 mg/ml), Naloxone (0.4mg/ml) and Antipamezol hydrochloride

(5mg/ml) in 0.9% NaCl for a final dose of 20ml/kg) was used and fully awaken animals were placed back in their cages and i.p injected with Buprenorphin (0.3mg/mL) for pain-relief.

Behavioral Tests

The Challenging Beam Test was performed using a beam with four 25 cm frames of progressively decreasing width as described before [20]. Animals were trained during 2 days to transverse the beam from the widest (frame 1) to the narrowest section (frame 4). On the test day, a mesh grid was placed over the beam leaving approximately 1cm space between the grid and the beam surface. Animals were video-recorded while crossing the grid-surface with five trials per animal. Frame 1 was excluded from the analysis due to variable reactions after first contact with the beam. Videotapes of each animal were rated for time to traverse the beam, number of errors and number of steps for each of the trials and averaged per animal.

The spontaneous activity on the Cylinder test was assessed as formerly [20]. Spontaneous activity in a glass cylinder was videotaped for 3-7 minutes and a test was considered valid if the number of rears were equal or > 20. To evaluate motor dexterity, the number of forelimb and hindlimb steps were counted. For vertical activity the number of rears were counted. Forelimb and hindlimb steps were counted when the animal placed a paw in a different position on the cylinder floor, towards a frontal or backwards movement. The percentage of total contralateral and ipsilateral steps, contralateral paw use and total forelimb and hindlimb steps were calculated. Detailed description can be found in supplementary information.

Perfusion and Tissue processing

Animals were euthanized with an overdose of pentobarbital (400mg/mL, 1:10 I.P.). Upon respiratory arrest, animals were transcardially perfused through the ascending aorta with ice-cold 0.9% NaCl solution, followed by 4% paraformaldehyde (PFA in 0.1M phosphate buffer, pH 7.4). PFA-perfused brains were removed and post-fixed in the same 4% PFA solution for 2h and transferred to a 25% sucrose solution (in 0.02M NaPBS) overnight for cryoprotection. Brains were subsequently sliced into 40-µm-thick coronal sections using a HM 450 Slicer Microtome (Brock and Michelsen, Thermo Fisher Scientific) and separated in series of 6 for the Striatum and of 4 for the SN. Sections were stored at -20°C in anti-freeze solution.

Immunohistochemistry with DAB detection and Immunofluorescence

Immunohistochemical staining was done on free-floating brain sections as previously described [19]. Briefly, sections were blocked in appropriate 5% normal serum and then labeled overnight with anti-tyrosine hydroxylase (TH, 1:750, Millipore), anti-aggregated α-syn MJFR-14-6-4-2 (MJF14,1:25000, Abcam), anti-phosphorylated α-syn (pSer129 α-syn 1:3000, Cell Signaling Technology), MHCII (1:400, eBioscience), p62/SQSTM1 (1:2000, Nordic Biosite), CD68 (1:1000, BioRad), Iba-1 (1:1000, Wako Fujifilm), GFAP (1:5000, Abcam), CD4 (1:500, BD Biosciences) or CD8 (1:500, eBioscience) in 2.5% serum and 0.25% Triton-X-100 in KPBS at room temperature. Sections were washed with KPBS, pre-blocked for 10min in 1% serum and 0.25% Triton-X-100 and incubated with the appropriate biotinylated secondary antibodies (1:200, Burlingame, CA Vector Laboratories) for 2 hours. Afterwards, avidin-biotin-peroxidase complex (ABS Elite, Vector Laboratories) was used and visualized using 3,3-diaminobenzidine (DAB) as a chromogen with 0.01-0.1% H_2O_2. Sections were mounted on chrome-alum gelatin-coated slides and coverslipped. For MHCII and Iba-1 staining, sections were counterstained with Cresyl violet (0.5% solution). Slides were analyzed using Leica DMI600B brightfield microscope unless specified.

For immunofluorescence, free-floating sections were blocked in the appropriate 5% normal serum and then labeled overnight with anti-TH (1:750, Millipore), anti-aggregated α-syn MJF14-6-4-2 (1:10000, Abcam), p62/SQSTM1 (C-terminus) (1:1000, Nordic Biosite) and Iba-1 (1:1000, Wako Fujifilm). Sections were washed with KPBS and incubated for 2 hours with species-specific fluorochrome-conjugated secondary antibodies (Alexa-Fluor 488 or 647, Invitrogen) plus DAPI (1:2000, Sigma-Aldrich A/S) for nuclear staining. Sections were mounted on chrome-alum gelatin-coated slides with Dako fluorescent mounting medium. Confocal images were obtained using a LSM 710 Meta Confocal microscope (Zeiss) with a 20X/0.8 M27 objective. Extraction of single z-frame and maximum intensity projections were performed with ImageJ (Fiji) software.

Densitometric analysis of dopaminergic axonal striatal innervation

Striatal density of TH+ dopaminergic fibers were measured by analysis of optical density at 6 different rostro-caudal levels [21]: AP: +1.10; +0.62; +0.38; +0.14; -0.22; -0.58 mm relative to bregma. Immunostained sections were scanned using a densitometer (EPSON Perfection 3200

(1800 dpi resolution, grayscale) and the digital images acquired were analyzed with ImageJ (Fiji) software using a grayscale. The optical density in each section was corrected to unspecific background measured in the corpus callosum of the same section. Data are shown as a percentage of the ipsilateral side vs. the contralateral side.

Stereology and microscopic analysis

Unbiased stereological estimation of total TH+ cells in the SN was performed by an observer blind to the animal's identity, using the optical fractionator principle [59, 82] using a Bright field Leica DM600B microscope and the NEWcast program (Visiopharm). A 1.25X low power objective (HCX PL Fluotar, Germany) was used to outline the SN based on its anatomical landmarks. Dopaminergic TH+ neurons were counted with a 40X objective (Leica, Germany) in a series of 1:4 sections covering the full SN (8-10 nigral sections per animal) from the rostral corner of the pars compacta to the caudal end of the pars reticulata (located between -2.70mm and -3.88mm from bregma [21]) with a counting frame of 56.89μm x 42.66 μm and a step length of 110-165 as to count a minimum of 100 cells per SN and a CE<0.1. Detailed description can be found in supplementary information.

Total number of cells with aggregated MJF14+ α-syn, and p62+ cells were manually counted in SN sections (three equally distant per staining; between -2.46 and -3.64 mm from bregma) [21]; CD4+ and CD8+ T cells were counted in striatal sections (three equally distant per staining; 1.18 and -0.22mm from bregma) using a Bright field Leica DM600B microscope. Enhanced Focal Images (EFI) captured using the Upright Widefield Slide Scanner microscope (UWSSM) were used to analyze the area covered by immunostaining in two coronal sections stained for: MJF14 aggregates in the amygdala and piriform cortex (between 0.26 and -2.18 mm from bregma); p62-expressing cells in the piriform cortex (-0.94 and -1.94mm); CD68 in the striatum (1.18 and -0.22mm); GFAP in the striatum (1.18 and -0.22mm) and in the SN (-2.70 and -3.88mm), using ImageJ (Fiji). Total number of MHCII+ cells in the SN were manually counted in a series of 6 equally distant midbrain coronal sections (-2.46 to -3.88 mm from bregma). MHCII+ expression in striatum the 1-month p.i. was qualitatively scored based on staining intensity and the area covered by immunostaining ranging from 0 (no staining) to 4 (intense and dense staining). At 6 months p.i, total number of MHCII+ cells in striatum were manually quantified in 3 equally distant coronal sections (1.18 and -0.22mm from bregma).

IBA-1: Iba-1+ cells were counted with a 40X objective in 3 equally distant SN sections (-2.70mm and -3.88mm) aided by the VIS module (Visiopharm program). The counting frame (56.89µm x 42.66 µm) was randomly located by the VIS module and methodically moved to sample the entire delineated region of the SN (step length of 75 µm) and all cells inside the counting frame were counted. A positive cell had a cresyl violet-stained nucleus covering a Iba1+ cell body. Four cellular profiles were defined as previously described [64]. The number of Iba-1+ cells per mm^2 was calculated according to the area sampled in each section (calculated by the VIS module) and the total number of cells counted per section. The percentage of each morphological cell type was calculated as total % of A,B,C and D type in each section and averaged per animal.

Brain cells isolation and fluorescence activated cell sorting for RNA isolation

Animals were transcardially perfused through the ascending aorta with ice-cold PBS, brain extracted and cells isolated using the Adult Brain Dissociation Kit (Miltenyi Biotec) in accordance with the manufacturer's protocol. Briefly, brains were cut into approximately 0.5 cm pieces and transferred into gentleMACS C Tubes containing the provided enzymes. Tissue was dissociated using the gentleMACS Octo Dissociator with Heaters for 30 min in the appropriate program. Homogenates were filtered through 70µm cell strainers and the cell suspension centrifuged at 300xg, 10 minutes at 4°C. Cells were resuspended in a Debris Removal Solution (in DPBS containing $CaCl_2$, $MgCl_2$, 1g/L D-Glucose and 36mg/L Pyruvate, Gibco) and centrifuged at 4°C and 3000xg for 10 minutes. Gradient centrifugation formed three phases and the top two layers containing myelin debris were removed. Cells were washed with 1x PBS and counted in the MOXI Z Mini Automated cell counter (ORFLO).

Freshly isolated brain cells were blocked with CD16/CD32 (clone 2.4G2, Mouse BD Fc block, BD Pharming) and 10% goat serum in PBS for 10min at 4°C. Single-cell suspensions were incubated in darkness at 4°C for 30 min with CD11b antibody conjugated to BV421 dye (50µg/mL, clone M1/70, BioLegend) and CD45 antibody conjugated to APC dye (0.2mg/mL, clone 30-F11, BioLegend). Cells were washed with PBS and 0.5% BSA, centrifuged at 4°C and 400xg for 5 minutes and resuspended in cold PBS. Propidium iodide (PI) was added to the cell suspension for identification of dead cells. Microglia and Macrophage populations were sorted into separate tubes containing PBS, in the FACSAria III high speed cell sorter (BD Biosciences,

San Jose, CA) according to CD11b (405nm laser and 450/40 bandpass filter) and CD45 (633nm laser and 660/20 bandpass filter) (**Suppl. Fig. 2**). Once sorted, microglia (200000-500000 cells) and macrophage (10000-30000 cells) cell suspensions (>90% purity after sorting) were centrifuged at 4°C and 400xg for 5 minutes, resuspended in RLT Plus Lysis buffer (QIAGEN, Germany) with 1% β-Mercaptoethanol and vortexed for 1 minute for cell lysis. The solution was further homogenized using a 1mL syringe and a 21gag needle. Total RNA was extracted using RNeasy® Mini Kit (QIAGEN) according to the manufacturer's protocol.

SMART-Seq2, gene mapping, expression and analysis

Total purified RNA was sent to BGI Hong Kong where Switching Mechanism at 5' End of RNA Template (SMART-seq2) sequencing service was requested. Samples were tested for quality control using Agilent 2100 Bio analyzer (Agilent RNA 6000 Nano Kit). RNA integrity (RNI) >7 was considered suitable for sequencing. Gene expression analysis was performed through full population RNA sequencing using the SMART-seq2 method according to BGI's standard methodology.

Reads mapped to rRNA were removed and raw data was obtained. The sequencing reads which contained low-quality, adaptor-polluted and high content of unknown base (N) reads processed were removed before downstream analyses. Clean reads were mapped to reference using Bowtie2 [38], and then gene expression level was calculated for each sample with RSEM [42], a software package for estimating gene and isoform expression levels from RNA-Seq data. Based on the gene expression level, we identified the DEGs (Differentially expressed genes) between α-syn PFF vs. MONO, Male vs Female, and WT vs. CD163KO groups. We use DESeq2 package of R [43] to detect the DEGs, determining at a cutoff of FDR corrected p-value≤0.05 and |log2(fold change)|≥1 as DEGs.

Principal component analysis (PCA) was performed on the Macrophage and Microglia population respectively based on the rlog of dds result from DESeq2 and draw the diagrams with ggplot2 function of R. Batch effect was corrected and three outlier samples were removed according to the results of PCA diagrams (**Suppl. Fig. 3**). With DEGs, we performed Gene Ontology (GO) and KEGG pathway classification and functional enrichment using the ClusterProfiler package of R [85]. GO has three ontologies: molecular biological function,

cellular component and biological process. We performed biological process and molecular biological function enrichment respectively, showed when relevant.

In vitro treatment of bone marrow-derived macrophages and gene expression analysis

Bone marrow derived macrophages (BMDMs) were prepared by flushing femur and tibia of CD163KO or WT mice, aged 6-12 weeks, with RPMI-1640. Flushed bone marrow was filtered through a 70 µm cell strainer (Corning®), and 6 x 10^6 cells were plated in uncoated petri dishes (Greiner Bio-one) in RPMI-1640 with 10% Fetal Bovine Serum (FBS, Biowest), penicillin and streptomycin and 2mM L-Glutamine (Gibco), supplemented with 10% L929 conditioned medium. Cells were supplemented with RPMI with 10% FBS, P/S, L-glut and 10% L929 medium at day 4, and on day 7 the cells were harvested with TrypLE (Gibco) and plated in 24 well plates for downstream assays. Plated BMDMs were incubated with 10 ng/ml IL-10 or IFNy (Peprotech) for 24 hours and subsequently stimulated with PBS control or 1µM murine α-syn PFF for 6 hours, after which the cells were lyzed in TRIdity G™ (Applichem). RNA was purified using the Direct-zol RNA kit (Zymogen), according to the manufacturer's protocol. The quantity and quality of the RNA was measured using a Nanodrop ONE (Thermo Fischer Scientific), and cDNA was prepared using the High-Capacity cDNA Reverse Transcription Kit (Applied Biosystems). qPCR was performed using the KAPA SYBR® fast low ROX (Sigma Aldrich), 5 ng RNA, and 0,4 µM combined forward/reverse primer on Applied Biosystems 7500 fast qPCR machine, and peptidylprolyl isomerase A was used as reference gene to calculate the relative gene expression ($2^{-\Delta\Delta Ct}$). See table in supplementary info for primers used.

Statistical analysis

All analysis were done by researchers blind to the group's identity. All statistical analysis were performed using GraphPad Prism v.8.4.3 (GraphPad Software, California, USA). Gaussian Normality was first assessed using normality distribution with a Shapiro-Wilk normality test followed by Two-way ANOVA and, when appropriate, by a post-hoc Sidak's multiple comparisons test. Three-way ANOVA with matched values was used when comparing contralateral and ipsilateral histopathological changes. Bonferroni corrections were applied when appropriate. Alpha was set at 5%.

RESULTS

α-syn PFF intrastriatal injection induced transient impairment in motor function in CD163KO males, but not in females.

To induce α-syn pathology, murine α-syn PFF (10 µg, 33.87nm of size), or monomeric α-syn as control, were injected into the right striatum. Based on our prior observations in humans with PD, we analyzed males and females separately. To evaluate whether the genetic deletion of the CD163 receptor would lead to differential sensorimotor behavioral changes after α-syn PFF intrastriatal injection, mice were assessed with the Challenging beam test at 1- and 6- months p.i. (**Fig. 1a-i and Suppl. Fig. 4**). At 1-month p.i., α-syn PFF CD163KO males showed a significant increase in the number of errors and errors/step when traversing frame 4 - the narrowest and most challenging frame - compared to WT and α-syn MONO CD163KO animals (**Fig. 1a-b**). An increase in total errors (summatory of frames 2-4) was also observed (vs. α-syn PFF WT males) (**Fig. 1c**). At this time point, no behavioral changes were found between the female groups (**Fig1. d-f**). The α-syn PFF injected CD163KO males showed significantly higher number of errors in frame 4 than CD163KO females (**Fig. 1h**), indicating a sex-specific role for CD163 in the early response to α-syn PFF. No relevant changes regarding time or number of steps were observed (**Suppl. Fig. 4a-d**). These behavioral changes were resolved after 6 months, when all groups showed similar motor behavior (**Suppl. Fig. 4c, d, e-f**).

Evaluation of the spontaneous activity in the Cylinder (**Fig. 1j-q**) at 1-month p.i. showed a general decrease in paw use - both in hindlimbs and forelimbs- in α-syn PFF CD163KO males (vs. α-syn PFF- WT males) (**Fig. 1k , Suppl. Fig. 5a**). However, at 6-months p.i., total paw use was similar across groups, while α-syn PFF CD163KO males showed a certain degree of asymmetry by using the contralateral hindlimb significantly less than α-syn MONO CD163KO (**Fig. 1l**). No difference was found concerning vertical activity (**Suppl. Fig. 5e, g, m, o**). Female mice showed no difference in the paw use or vertical activity at any time-point (**Fig. 1n-q, Suppl. Fig. 5b-h, j-p**).

Increased α-syn pathology in the brain of CD163KO females.

We then analyzed the α-syn pathology in the brain using two antibodies: the MJF14 (**Fig. 2a, Suppl. Fig. 6**), which preferentially binds a conformational specific epitope in aggregated α-syn

[16, 39, 74]; and another against phosphorylated α-syn at Ser129 (pSer129), which is enriched in PD brains [23]. At 1-month-p.i., MJF14+ α-syn pathology was present in all regions evaluated (Striatum, Piriform Cortex, Amygdala, Thalamus and SN) in the ipsilateral hemisphere, and mostly prevalent in neuropil-like structures putatively associated with axonal/neurite aggregates (**Suppl. Fig. 6**). Quantification of the MJF14 staining revealed no significant differences between groups at this time point (**Fig. 2b-d**). After 6 months, the α-syn MJF14+ immunostaining was increased and appeared in numerous cell-body-like structures (**Fig. 2a**). CD163KO females showed significantly higher MJF14+ staining in the piriform cortex and amygdala (**Fig. 2e-f**), and a similar trend in the number of MJF14+ cell bodies in the SN (p=0.055) (**Fig. 2g**). Positive immunostaining against pSer129 was detected in the same brain regions and revealed hyperphosphorylation in all PFF injected animals but particularly in CD163KO females (**Fig.2a, lower panel**). Our results suggest a role for CD163 in the brain's ability to avoid/handle α-syn pathology, with particular relevance for females.

The progressive pathological α-syn inclusion burden is associated with p62 accumulation

To evaluate the autophagic system we performed immunohistochemistry against p62/SQSTM1, as increased p62 immunostaining is widely used as a marker for autophagic flux inhibition [33]. We observed p62 accumulation in the ipsilateral SN 1 month p.i. in all groups (**Fig. 3a-c**), but significantly less in α-syn PFF CD163KO females vs. WT females (**Fig. 3a-b**). However, at 6-months p.i., while p62+ cells in SN decreased in most of the PFF injected animals, this was not seen in α-syn PFF CD163KO females that tended to have more p62 signal than WT females (p=0.08) (**Fig. 3d-e**), suggesting a delayed failure of the autophagic systems in this group. This autophagic failure was associated with α-syn pathology, since the number of MJF14+ cells in SN were significantly correlated with the p62+ cells in all α-syn PFF injected animals (p=0.057 at 1-month (**Fig. 3c**) and p=0.002 at 6 months p.i. (**Fig. 3f**)).

At 6 months p.i., p62 staining in the piriform cortex was specifically increased in α-syn PFF CD163KO females (**Fig. 3g-h**), found again strongly associated with the increased MJF14 α-syn pathology, which was given by a significant correlation mostly driven by the CD163 deletion in females (**Fig. 3i**). Confocal analysis of p62 and MJF14 in the different brain areas at 6 months p.i. revealed that some, but not all, p62 cellular structures co-localized with aggregated α-syn (particularly cytoplasmic aggregates of half-moon shape) (**Fig. 4**). Altogether, our data suggest

that the lack of CD163 results in changes in the α-syn induced failure of the p62-mediated autophagic degradation in a sex-specific manner.

Differential microglia and astrocytic responses to α-syn PFF injection in CD163KO females

Since the immune response in the CNS involves astrocytes and microglia, we evaluated both populations (**Fig. 5a-m**) [69]. At 1 month p.i. ipsilateral GFAP astrocytic expression was increased in the striatum of all α-syn PFF-injected groups, except in CD163KO females, which appeared similar to α-syn MONO-groups (**Fig. 5b, d**). This suggests an early impaired astrocytic response by CD163KO females. No significant differences were found in the SN at this time-point (**Fig. 5e**), nor after 6 months in any brain region. (**Fig. 5g-h**). Co-staining of GFAP and p62 did not reveal any co-localization, suggesting that overt inhibition of autophagic flux is not occurring in astrocytes (**Suppl. Fig.7a**).

No significant differences in the number of Iba1+ microglia were found in the SN of the male groups (**Fig. 5k, m**), however, we found an ipsilateral Iba1+ cell proliferation in α-syn PFF CD163KO females (vs. α-syn PFF WT and vs. α-syn MONO CD163KO females) (**Fig. 5j, l &m**). Co-staining of Iba-1 and p62 did not reveal any detectable inhibition of autophagic flux in microglia (**Suppl. Fig.7b**). Analysis of the microglia morphology revealed a decrease in the percentage of Iba-1+ type A cells (homeostatic) in the ipsilateral side of α-syn PFF WT and CD163KO males (vs. contra) that was mirrored by an increase of the other more activated profiles (**Suppl. Fig. 8a**). This was also true in the ipsilateral side of α-syn PFF WT females (vs. contra & ipsi α-syn MONO-injected), but not in CD163KO females (**Suppl. Fig. 8b**), suggesting a dysfunctional microglia response to α-syn PFF injection in females lacking CD163.

CD68 expression was used as an indirect measurement of phagocytic activity in immune cells (**Fig. 5a**). At 1 month, α-syn PFF injection led to a significant increase in CD68 staining in both males and females compared to α-syn MONO injection (**Fig. 5c**). However, this increase in CD163KO females was only a trend (p=0.0524), and it was of a lesser extent than those observed in the other α-syn PFF groups (**Fig. 5c**). Interestingly, both CD163KO males and females showed CD68+ cells of bigger size and shorter ramifications, suggestive of a highly activated/phagocytic phenotype (**Fig. 5a**). At 6 months p.i., CD68 expression decreased to those observed in the MONO groups in all PFF groups (**Fig. 5f**, **i**). In conclusion, the lack of CD163

receptor resulted in an early differential microglia response in females, together with a parallel absence of astrocytic response to α-syn PFF injection.

Robust upregulation of MHCII expression in α-syn PFF injected males

Expression of MHCII is a widely used marker of activated microglia, and has been associated with α-syn pathology in rodent models [64] and in *postmortem* PD brains [49]. MHCII expression, which is rarely found in microglia in the healthy brain, was observed upregulated early in the same anatomical regions where MJF14/pSer129+ α-syn pathology were present (**Fig. 6a**). In most brain regions, the MHCII+ cells exhibited a ramified morphology (likely microglia), however, in the piriform cortex, we only observed numerous elongated rod-shape MHCII+ cells, resembling perivascular macrophages (**Fig. 6a)**. At 1-month p.i., MHCII expression in the ipsilateral striatum was the highest of all examined areas, but α-syn PFF CD163KO females presented the lowest expression signal, whereas most of the CD163KO males show higher MHCII expression (**Fig. 6c**). At this time point, MHCII+ ramified cells in the ipsilateral SN were significantly higher in all α-syn PFF male groups compared to MONO-injected animals. Interestingly, only a few cells expressed MHCII in the female groups, even though α-syn PFF CD163KO females showed the highest number (**Fig. 6b**). MHCII expression levels declined after 6-months p.i., where animals rarely presented MHCII-expressing cells in the SN (**Fig. 6d**). This was also true for the striatum, except for α-syn PFF CD163KO females that showed significantly higher number of MHCII+ ramified cells (vs. α-syn PFF WT females), even though still at a low degree (**Fig. 6e**). Therefore, the absence of CD163 resulted in a differential MHCII+ response to α-syn pathology, in a sex-dependent manner.

CD163KO females show dysfunctional CD4 and CD8 T cell responses to α-syn PFF injection

As altered innate immune responses will influence the adaptive immune system, and since both CD4 and CD8 T cells have been observed in *postmortem* PD brains, we studied the T-cell brain infiltration in the striatum (**Fig. 7**). The injection of α-syn PFF in WT male and female mice lead to early ipsilateral infiltration of CD8+ T cells that was not observed in the MONO injected groups. However, infiltrated CD4+ T cells were equally observed both in the ipsilateral striatum of α-syn PFF- and the MONO injected animals (**Fig. 7a-c**), and particularly α-syn MONO-

injected WT males, which showed a bilateral T cell infiltration (**Fig. 7b**). In agreement with our MHCII observations, T cell infiltration, both CD4+ (**Fig. 7a-b** vs. MONO and vs. contralateral) but also CD8+ (**Fig. 7a, c**, vs. MONO, vs. WT, vs. contralateral and vs. CD163KO females) were enhanced in α-syn PFF injected CD163KO males 1 month p.i. However, at this time-point, CD163KO females showed impaired CD4+ and CD8+ T cell responses upon α-syn PFF injection. Thereafter, at 6 months p.i, despite the overall decrease in T cell numbers, both WT and CD163KO males still showed an increase in ipsilateral CD8+T cells (**Fig. 7e**, vs. contralateral), while no significant CD4 infiltration was seen (**Fig. 7d**). In contrast, in the female group, only α-syn PFF CD163KO showed infiltrated CD8+ T cells (**Fig. 7e**, vs. WT and vs. contralateral) and a similar trend for CD4+ T cells in the ipsilateral striatum was observed (**Fig. 7d**, p=0.052 vs. contralateral). These observations suggest a role for CD163 in modulating innate immune responses and in turn adaptive immune responses to α-syn PFF injection, in a sex-specific manner.

Lack of CD163 in females results in enhanced nigro-striatal dopaminergic neuronal loss induced by α-syn PFF injection

Given our observations on the alteration of α-syn pathology and sex-specific dysfunctional immune responses in the absence of CD163 receptor in monocytes/macrophages, we sought to determine if this would lead to distinct neurodegenerative events (**Fig. 8**). Densitometry analysis of striatal TH+ fibers revealed a 18-21% decrease in the ipsilateral axonal fibers in all α-syn PFF groups at 1 month p.i. (vs. α-syn MONO control) (**Fig. 8a-b**), which remained after 6-months, in α-syn PFF males (**Fig. 8c-d**). However, α-syn PFF CD163KO females show a further reduction to 44% in TH+ ipsilateral fibers, significantly lower than both α-syn MONO CD163KO and α-syn PFF WT females (**Fig. 8e-f**). No particular rostro/caudal pattern of dopaminergic fiber loss was seen (**Fig. 8d,f**).

Stereological quantification of TH+ cell bodies in the SN did not reveal any significant cell loss after 1 month (**Fig. 8g-h**), however, after 6 months, WT and CD163KO α-syn PFF males showed a 33% and 38% loss of dopaminergic neurons respectively in the ipsilateral SN (vs. α-syn MONO injection) (**Fig. 8i-j**). Notably, α-syn PFF CD163KO females showed the biggest ipsilateral loss of dopaminergic neurons (54%) compared to α-syn MONO CD163KO and WT α-syn PFF females (**Fig. 8k,j**); but also to CD163KO α-syn PFF males ($F(1,29)=7.515$, $P=0.0104$), $p=0.07$ after post-hoc analysis) (**Fig. 8n**). The total number of ipsilateral TH+ neurons was

significantly reduced in all α-syn PFF injected animals (vs. contralateral side and ipsilateral α-syn MONO) (**Suppl. Fig. 9a-b**).

As expected, the striatal axonal TH+ density correlated significantly to the number of TH+ neurons in the SN (**Fig. 8l**). In α-syn PFF groups, this correlation was observed in both males and females (**Suppl. Fig. 9c, f**), particularly in females WT, where a strong association was seen (**Suppl. Fig. 9g**). However, CD163KO females lacked this association (**Suppl. Fig. 9h**), suggesting an irregular, dysfunctional response in the disease progression. These data suggest a sex-dependent neuroprotective role for the CD163 receptor in the progressive neurodegenerative process triggered by α-syn aggregation.

p62 neuronal aggregates and α-syn pathology are associated with cell death and motor impairment in CD163KO males.

Since autophagic dysfunction has been proposed to be a core event in the PD neurodegeneration, we investigated the association between p62 accumulation with the histological and behavioral changes observed in the animals. Confocal imaging confirmed that p62+ accumulation is present in the cytoplasm of TH+ dopaminergic neurons (**Suppl. Fig. 10a, arrowheads**), suggesting that inhibition of autophagic flux occurs in neurons. Moreover, the number of p62+ cells in the SN negatively correlated with the percentage of surviving TH+ SN neurons in α-syn PFF injected animals (**Suppl. Fig. 10b-h**). This correlation was stronger in males (**Suppl. Fig. 10c**) and particularly driven by CD163 deletion (**Suppl. Fig. 10e**), suggesting that p62 accumulation is a significant factor in driving neurodegeneration in CD163-deficient males.

When correlating motor behavior markers with the pathological readouts, we observed that the number of errors/step on frame 4 of the challenging beam was negatively correlated with the number of MJF14+ cells and the number of TH+ neurons in the SN of WT α-syn injected males (**Suppl. Fig11a-b**), but positively correlated to the amount of α-syn-MJF14 pathology in the SN in CD163KO males at 1 month p.i. This suggests that α-syn aggregation could partially explain their motor impairment (**Suppl. Fig. 11c-d**). Furthermore, at 6 months p.i., the use of the contralateral affected hindlimb of CD163KO males in the cylinder test decreased with reduced numbers of TH+ cells (**Suppl. Fig. 11e**) and increased p62+ aggregates in the SN (**Suppl. Fig. 11f**). Therefore, α-syn accumulation, autophagy impairment and SN neuronal death contribute to the motor defects seen in CD163-deficient males.

Notably, in females but not in males, the loss of dopaminergic axons significantly correlates with both MHCII and CD68 expression in the striatum at 6 months p.i (**Suppl. Fig. 12a-f**). These observations, together with the striatal MHCII and nigral Iba-1 increase in CD163KO females 6 months p.i suggest that, in females, the degenerative process is potentially driven by the immune events.

CD163 deletion alters the gene expression profile of macrophages and microglia after α-syn PFF injection

In order to further comprehend the consequences of CD163 absence in the immune response in the brain of the females, we performed SMART-seq2 at 2 months p.i on two FACS-sorted brain immune populations expressing: CD45 low/intermediate/CD11b$^+$ (Microglia) and CD45 high/CD11b$^+$ (macrophages (brain border associated and infiltrated), neutrophils and NK cells), which we refer to as the Macrophage population (**Fig. 9**). This time-point was chosen to secure that the observations were related to the pathology induced by the α-syn neuronal accumulation and not to the surgery or the extracellular presence of α-syn PFF. Analysis of the DEGs revealed a reduced ability of the macrophage population to respond to α-syn PFF injection (vs. α-syn MONO) in the absence of CD163 in females. This was paralleled by a differential response of the microglia population to α-syn pathology when comparing with the WT (**Fig. 9a**). In the two populations, very few or no DEG were commonly shared between WT and CD163KO females, suggesting that CD163 deficiency drastically affects the immune response to the α-syn pathology in the mice (**Fig. 9b**).

Within the macrophage population, the most upregulated genes in WT females were related to DNA damage response and regulation of catabolic processes (*Cecr2, Fzd6*), while genes associated with amino acid/protein metabolism (*Mpst, Akr1c12, Rsc1a1, Zfp354c*) and cytoskeleton organization (*Frmd5, Fhod3*) were found downregulated (**Fig.9c**). Remarkably, CD163 deletion in females resulted in a drastically reduced macrophage response to α-syn PFF, suggestive of impaired ability to form an otherwise “normal” response to the aggregated protein. Enriched gene ontology (GO) functional annotations showed that the downregulated genes in the females CD163KO were involved in regulation of calcium homeostasis and metabolism (**Fig. 9d,g**), known to play a central role in immune cell activation [77]. The microglia population of the α-syn PFF injected WT females showed upregulation of genes related to: peptide delivery to

MHCI (*Lrmp*) and regulation of TLR4 surface expression (*Cnpy4*). On the contrary genes associated with: vesicle coating (*Clvs1*), DNA repair (*Mcm8, Trib2*) and metabolic mechanisms (*Got1l1, Acot11, Kyat1*) were downregulated (**Fig.9e**). Interestingly, microglia from CD163KO females revealed the most significant DEGs (lowest p value and highest fold change (PFF vs MONO). Here, we saw upregulation of *Lnx1*, a gene related with ubiquitination and activation of proteosomal degradation mechanisms, *St8sia1,* associated with sphingolipid metabolism, and *Ptprcap,* a protein-coding gene that functions as a key regulator of CD45-CD4 T-cell interaction through the TNFR1 pathway. Genes related with DNA damage response (*Atad5, Smad9*), apoptosis modulation (*Dab2ip*), cell migration (*Dnai3*) and cytoskeleton organization (*Slain1*) were found downregulated (**Fig.9f**).

Since CD163KO females showed a significant increase in α-syn-mediated neurotoxicity, we further focused on this group and assessed the response to α-syn PFF and α-syn MONO in CD163KO vs. WT females. The number of DEGs in α-syn PFF-CD163KO female macrophages were significantly reduced when compared to α-syn MONO females (Fig.10a) and were once again associated with downregulation of genes related to amino acid/protein metabolism (*Nanp*), cytoskeletal dynamics (*Fam171a1*) (as seen vs. α-syn MONO), tight junctions and BBB integrity (*Cldn10*) (**Fig.10b**. Microglia gene expression was also affected by macrophage dysregulation (Fig.10a), with downregulation of iron metabolism-related genes (*Heph*), and heparan sulfate biosynthesis mechanisms (*Hs3st5*). Moreover *Ccl22,* a chemokine related to T-cell migration was also downregulated in CD163KO females, suggesting that CD163 expression in myeloid cells influences peripheral cell infiltration in females. GO analysis revealed few specific pathways affected by gene downregulation, and were limited to ubiquitin binding and DNA catalytic activity pathways (not shown). The most upregulated genes were: *Ntf3* which encodes Neurotrophin3, a protein involved in neuronal survival and differentiation, and, once again, *Lnx1* and *Ptprcap* (**Fig.10c**). Interestingly, STRING analysis of the Ptprcap protein shows interaction with CD4, TNFR1 and TWEAK pathways (**Fig.10d**). Altogether, these results suggest that the early transcriptomic immune alterations seen in CD163KO females may contribute to their higher susceptibility to α-syn PFF.

To investigate potential sex-differences, we compared DEGs in Males vs. Females after α-syn PFF injection (**Fig.10e-g**). Macrophage transcriptomic changes were very different

between sexes in the WT group, where, in contrast to females, males presented highly downregulated genes related to modulation of epigenetic machinery and DNA repair mechanisms (**Fig.10f**), confirming a sex-dimorphism in the macrophage response to α-syn PFF. Remarkably, this sex difference in DEGs was lost upon CD163 deletion, which mostly resulted in a few downregulated genes in male macrophages (**Fig.10e**). However, the lack of CD163 resulted in a bigger number of genes differentially regulated in male microglia (vs. females), also compared to those in the WT group (**Fig.10e**). The most highly upregulated gene found in CD163KO male microglia (vs. female) was *Pacrg*, which encodes the Parkin co-regulated protein, a protein found in LBs [72] and related to aggresome formation and increased autophagy [71]. Confirming our previous observations, the most significant downregulated genes in CD163KO male microglia were *Lnx1* and *Ptprcap*, which, as mentioned, were the most upregulated genes in CD163KO females (vs. WT and vs. MONO) (**Fig.10g**). These results confirm the sex-specific role for the receptor in the α-syn-associated immune response.

CD163 deletion does not alter the pro-inflammatory gene expression profile of bone marrow-derived macrophages after *in vitro* stimulation and α-syn PFF treatment

To evaluate if CD163 deletion in macrophages would affect the cellular response to α-syn PFF *in vitro,* we isolated BMDM from WT and CD163KO mice and stimulated them with either IL-10 or IFNγ for 24h prior to α-syn PFF treatment (**Suppl. Fig13**). qPCR analysis showed an increased gene expression of Cxcl10, TNF and iNOS after BMDM priming with IFNγ, which was significantly enhanced by α-syn PFF treatment in both WT and CD163KO males (**Suppl. Fig13a,c-d**) and females (**Suppl. Fig13e,g-h**). IL-1β expression, was significantly increased in all WT mice and CD163KO males BMDM primed with IFNγ and incubated with α-syn PFF (**Suppl. Fig13b,f**); but not in CD163KO females BMDM (**Suppl. Fig13f, red bars)**, suggesting an irregular response to α-syn PFF. Expression of VCAM-1 and VEGFR1 (*Ftl-1*) mRNA were also measured, but no differences between groups were seen (not shown). Thus, the absence of CD163 does not drastically affect the ability of monocytes to respond to fibrillar α-syn-mediated inflammation and activation.

Discussion

To investigate the involvement of CD163 in the α-syn induced neurodegeneration and associated immune response, we injected α-syn PFF or MONO in the striatum of CD163KO or WT mice. Based on prior observations in humans with PD, sexes were analyzed separately. α-syn PFF injection resulted in early and sustained motor alterations in CD163KO males, but not in females. However, α-syn PFF injection led to a progressive α-syn pathological accumulation and autophagic failure -p62 accumulation- being significantly higher in CD163KO females after 6 months. α-syn PFF-injections resulted on early immune response, with upregulation of CD68, MHCII, T-cell infiltration and astrogliosis, that was lower or absent in CD163KO females. Nevertheless, this group revealed a delayed but significant immune response at 6 months as shown by the Iba1+ microglia proliferation in SN, and the highest MHCII expression, and T-cell infiltration in striatum. Remarkably, this differential immune response and the increased pathological α-syn observed in CD163KO females culminated in higher nigrostriatal dopaminergic degeneration. Correlation analysis showed that α-syn pathology, autophagy impairment and neuronal death may be partial contributors to the motor defects seen in CD163KO males, while in females, the dopaminergic degeneration was significantly associated with the immune events. RNA-seq analysis revealed that CD163KO female macrophages lack the ability to respond to α-syn PFF. Additionally, CD163KO in females induced an altered microglial phenotype with upregulation of genes related to pro-inflammatory pathways, which, together with changes in the intracellular milieu, may contribute to the enhanced α-syn PFF-induced neurodegeneration observed in CD163KO females. Overall, our data support a novel and sex-dependent role for CD163 in the α-syn-induced immune response and neurodegeneration.

The intra-striatal injection of murine α-syn PFF lead to the aggregation of the endogenous α-syn and α-syn pSer129 accumulation in anatomically connected areas as seen before [22, 45, 56]. This was prominent in CD163KO animals and particularly enhanced in CD163KO females. Ser129 phosphorylation has been associated with α-syn toxicity *in vivo* [23] and *in vitro* [66]. Thus, CD163 genetic deletion potentiates α-syn misfolding and phosphorylation, which increases the formation of highly toxic α-syn aggregates, particularly in females. α-syn aggregation and neuronal toxicity is associated with autophagic dysfunction and p62 accumulation [46]. Accordingly PFF-injected mice showed p62 accumulation that paralleled the α-syn PFF pathology; and thus, although delayed compared to the other groups, it was higher in CD163KO

females at 6 months. Therefore, CD163 absence resulted in a more prominent long-term autophagic failure in females. p62 has been recently suggested to be required for the synucleinophagy in microglia, i.e. the engulfing of α-syn into autophagosomes for degradation via selective autophagy [10]. Although the highest p62 accumulation coincided in time with the increased Iba1+ microglia in the SN in CD163KO females, we did not find p62 accumulation in glia. However, p62 colocalized with MJF14+ α-syn aggregates, and it was observed in SN dopaminergic neurons in agreement with our prior observations in the rat PPF PD model [74]. Interestingly, we have recent *in vitro* observations showing that sCD163, an extracellular protein produced during monocyte activation, increases the uptake of extracellular α-syn by monocytes and microglia [53]. Our results here may therefore suggest that CD163 deficiency may compromise the ability of myeloid cells to properly respond to α-syn, consequently promoting its pathological intraneuronal accumulation and autophagy failure. Altogether, the absence of CD163 led to a more prominent α-syn pathological accumulation and collapse in the autophagic system, particularly in females in the long term.

PD related inflammation involves both brain and peripheral immune cells [27]. Accordingly, the α-syn-PFF PD model shows neuroinflammation with microgliosis [13, 74], CD163 macrophages infiltration in rats [26] and changes in peripheral immune cells in mice [15, 24, 25]. Indeed, we observed increased CD68 expression suggestive of an early phagocytic microglia activation, which coincided with MHCII upregulation. This MHCII response was higher in the CD163KO males, suggesting an enhanced early adaptive immune activation, as confirmed by the higher CD4 and CD8 T-cell infiltration. In contrast, this early immune response was not seen in the α-syn PFF CD163KO females, which also lacked the astrocytic GFAP upregulation seen in all other PFF-injected animals. However, after 6 months, when this immune response was resolved in all groups, it became relevant in the α-syn PFF CD163KO females, which showed a significant unique microgliosis (Iba-1+ proliferation) in the SN, higher MHCII expression and CD4 and CD8 T cell infiltration in the striatum. This might ultimately contribute to higher neurodegeneration as adaptive immunity and T-cells have been shown to mediate dopaminergic loss in PD models [8, 83]. In conclusion, CD163-deficient females showed an inability to timely respond to early α-syn-associated pathological events, which resulted in delayed but long lasting neuroinflammation involving both innate and adaptive cells.

Further corroborating a differential immune response, our transcriptomic data confirmed that CD163 deficiency leads to macrophage impaired responses to α-syn PFF in females that in turn modified the microglia response. Most DEG in the female CD163KO macrophages were downregulated and involved in different processes such as: amino acid/protein metabolism and calcium homeostasis regulation, which plays a central role in immune cell activation [77]. Also, others related to cytoskeleton organization, BBB integrity and immune cell transmigration, which could be associated with the early decreased T-cell infiltration in this group. α-syn PFF-injected WT female microglia showed upregulated genes coding for proteins previously related to α-syn immune response (MHC system and TLR4). However, microglia from CD163KO females showed downregulation of *Ccl22*, a chemokine involved in regulation of leukocyte migration [11] that might also contribute to the decreased T-cell infiltration. This may suggest that CD163 expression is involved in the early peripheral cell infiltration in females.

Of particular interest in CD163KO females, we observed upregulation of *Ptprcap*, a key regulator of CD45-CD4 T-cell interaction and activation [41], also associated with activation of the TNFR1 and TWEAK pathways. Interestingly, sCD163 is suggested to act as a decoy receptor for TWEAK and regulate TWEAK-induced pro-inflammatory canonical NF-κB activation [2]. Microglial TWEAK production decreased synaptic plasticity and promoted phosphorylation of pre- and post-synaptic proteins in an AD mouse model [51]. Notably, TWEAK has been associated with dopaminergic cell death and the pro-inflammatory activation of astrocytes in the MPTP PD model [50, 63], and TWEAK is increased in PD patients' serum [62]. Therefore, upregulation of *Ptprcap* and possible TWEAK-mediated inflammation may be also involved in the higher CD163KO females' susceptibility to α-syn PFF.

The higher burden of α-syn pathology and the differential immune response observed in the α-syn PFF CD163KO females resulted in increased nigral dopaminergic loss. Infiltration of peripheral immune cells such as, macrophages, NK cells or T cells into the brain will influence the microglia response and positively or negatively affect neuronal health [14, 27]. CD163+ cells infiltrate the brain in the 6-OHDA [73] and the α-syn PFF rat model [26, 74]. CD163+ cells are also found in PD *postmortem* brains [58]. Increased CD163+ cell numbers and CD163 expression levels (in both sexes) were paralleled by an increase of the migration markers CCR2 and CD11b on monocytes from blood of patients with early PD (<5 years from diagnose) [34]. Moreover, we have shown that shedding of CD163 is elevated in the CSF from PD patients and

associated with cognitive symptoms and levels of well-characterized neurodegenerative markers such as α-syn and Tau [53]. Therefore, CD163+ monocytic activation in the brain, and thus loss of the membrane CD163, is associated with neuronal dysfunction and related to cognitive ability. Our data here supports a protective role for the CD163 receptor on myeloid cells. This is agreement with our recent observations in REM sleep behavior disorder patients (prodromal PD), where higher numbers of CD163 cells in the blood were associated with lower immune activation in the SN and better dopaminergic transmission in the putamen as shown by positron emission tomography imaging [18], which indicates an overall protective role for CD163+ cells in prodromal disease stages. Intriguingly, we observed here that CD163 neuroprotective role seems especially relevant in females. Remarkably, we have previously seen that shedding of CD163 was only increased in the sera from female PD patients, but not in males, supporting a sex-difference regarding the CD163-system/cells during PD [53]. Further suggesting a sex-dimorphism in the PD associated immune response, blood CD14+ monocytes transcriptome differs between male and female PD patients [7]. Our RNA-seq analysis of the immune response to α-syn PFF in WT animals further corroborates a sex-dimorphic immune response, which may have consequences in the neuronal fate. Sex differences in immune cells have been described before [32], with new evidence of sex-distinct monocyte aging [47]. Microglia in females showed a higher anti-inflammatory capacity [78] and peripheral immune cells in males presented an accelerated inflammatory/aging signature [48]. The observed differential behavior of the CD163 and dimorphic immune response might be related to the higher PD risk associated with the male sex [76] and the differential presentation of the disease among sexes [28]. Our data suggest that the CD163 receptor is also involved in this immune sex-dimorphism, as its deletion in females resulted in a defective ability of immune cells to properly respond to the initial α-syn pathological effects, ultimately influencing the long-term degenerative outcome, while in males the absence of the CD163 receptor increased motor defects.

Our behavioral analysis points towards a relevant role for the immune system in the symptomatic presentation of the disease. α-syn PFF CD163KO male animals showed first a transitory decreased sensorimotor coordination, and later an asymmetric paw use. This was not seen in CD163-deficient females, which also point towards a sex-difference in the symptomatic manifestation of motor defects ultimately influenced by the immune environment. The lack of CD163 has been associated with distinct temporal influences on neurobehavioral tests and

mortality in a mouse model of intracerebral hemorrhage [40]. However, this study included only males and shorter time-points. CD163 deficiency has also been reported to strongly enhance severity and lead to imbalanced Th1/Th2 responses in a model of rheumatoid arthritis [68]. Interestingly, despite the α-syn pathology and the dopaminergic degeneration seen in WT, we only observed behavioral changes in the CD163KO mice, thus supporting a role for the immune environment in motor performance. Indeed, we and others have previously reported that the α-syn PFF PD model (male or female) do not exhibit robust motor defects despite the nigral degeneration [54, 55, 74]. Such observation suggests that the immune response has a significant influence in the motor manifestation of the disease. This might be exerted by soluble cytokines [67, 81] or peripheral cell infiltration, which can potentially influence microglia and neuronal function/firing [3]. Accordingly, sickness behavior was associated with peripheral inflammation responsible for sensorimotor defects [84]. Together with the observed early increase in MHCII immune activation and the CD4 and CD8 T cell infiltration, the behavior impairments in CD163KO males could also be partially contributed by the neuronal α-syn pathology, autophagic failure and, of course, nigral dopaminergic cell death, as suggested by the significant association of these markers with motor defects. Interestingly, in females but not in males, we found that loss of dopaminergic fibers significantly correlates with both MHCII and CD68 expression in the striatum 6 months p.i. These observations, together with the late striatal MHCII immune activation, T cell infiltration and nigral Iba-1+ cell proliferation in CD163KO females, suggest that the degenerative process is potentially driven by the long-lasting immune events.

Overall, our results suggest that, although CD163 deletion does not affect the *in vitro* acute monocytic response to fibrillar α-syn-induced activation, *in vivo* it results in a differential early transcriptomic innate immune response. In males, CD163 deletion leads to early increased T-cell infiltration and motor impairment, while in females it may contribute to their higher susceptibility to α-syn PFF and promote the increased long-term neurodegeneration. Interestingly, CD163 expression is described in the disease associated microglia (DAM) in AD [9]. According to scRNA studies, CD163 is not found in homeostatic microglia [5, 29, 31], thus its expression in the DAM might indicate an ectopic expression, or as suggested before, a loss of identity of the microglia during disease that downregulates its characteristic markers while gaining others [30, 36]. Therefore, is difficult to clearly conclude if the DAM population is

indeed microglia or it might include de-differentiated infiltrated macrophages. Notably, in a recent scRNA-seq study in the brain from PD patients also highlighted CD163 expression in the DAM response [65]. Moreover, in AD, the subpopulation of CD163+ amyloid-responsive microglia were depleted in AD cases with APOE and TREM2 risk variants, suggesting a protective role [52]. Moreover, CD163 upregulation has been also associated with macrophages with neuroprotective capacity in an AD model [35]. Thus, it could be speculated that CD163 upregulation in brain is associated with a protective compensatory mechanism exerted by myeloid cells as it also occurs in the blood monocytes in PD patients [34]. In conclusion, we demonstrate for the first time that the α-syn-associated innate immune responses involving CD163 expression differs between males and females, suggesting that the sex-dimorphism in PD may be due to immune differences. Therefore, future designs of immunomodulatory treatments should account for distinct immune phenotypes. In addition, our data suggest that upregulation of CD163 in the myeloid response during neurodegenerative disease seems to be a compensatory neuroprotective mechanism. Further studies are needed to fully understand CD163 role during brain diseases and the associated molecular mechanisms.

ACKNOWLEDGEMENTS

We are grateful to the FACS core facility for the technical help with the FACSAria III high speed cell sorter and the Imaging core facility for technical support with the Upright Widefield Slide Scanner microscope. Funding support for the research covered in this article was provided by the Bjarne Saxhof Fund administered through the Danish Parkinson's Foundation (MRR), the Novo Nordisk Foundation (DEO, NNF17OC0028806, MRR) and Independent Research Fund Denmark (9039-00217B, MRR). The Lundbeck Foundation grants R223-2015-4222 and R248-2016-2518 for Danish Research Institute of Translational Neuroscience-DANDRITE for PHJ and CB. SAF was a recipient of a PhD fellowship from the Graduate School at the Health Faculty, Aarhus University when performing the experiments described here.

AUTHORS CONTRIBUTION

SAF and MRR performed stereotaxic surgeries; SAF, IK and AK performed and analyzed behavior studies and histological samples. GUT processed brains for histology and SAF and GUT performed immunohistochemistry, SAF performed microglia/macrophage isolation, selection and RNA purification; RKR performed qPCR analysis; CL and YL analyzed the SMARTseq2 data. AE, PS, and SKM generated the CD163KO mouse line. CB and PHJ produced the recombinant mouse α-syn PFF. MRR conceived the idea, SAF and MRR designed the study and wrote jointly the final version of the manuscript. All authors contributed to the manuscript and approved the final version.

CONFLICT OF INTEREST

S.K.M. owns shares in Affinicon, which holds IP protecting the use of CD163 drug targeting. The remaining authors declare no competing financial interests.

REFERENCES

1 Abdelmotilib H, Maltbie T, Delic V, Liu Z, Hu X, Fraser KB, Moehle MS, Stoyka L, Anabtawi N, Krendelchtchikova Vet al (2017) α-Synuclein fibril-induced inclusion spread in rats and mice correlates with dopaminergic Neurodegeneration. Neurobiol Dis 105: 84-98 Doi 10.1016/j.nbd.2017.05.014

2 Akahori H, Karmali V, Polavarapu R, Lyle AN, Weiss D, Shin E, Husain A, Naqvi N, Van Dam R, Habib Aet al (2015) CD163 interacts with TWEAK to regulate tissue regeneration after ischaemic injury. Nature Communications 6: 7792 Doi 10.1038/ncomms8792

3 Badimon A, Strasburger HJ, Ayata P, Chen X, Nair A, Ikegami A, Hwang P, Chan AT, Graves SM, Uweru JOet al (2020) Negative feedback control of neuronal activity by microglia. Nature 586: 417-423 Doi 10.1038/s41586-020-2777-8

4 Barkholt P, Sanchez-Guajardo V, Kirik D, Romero-Ramos M (2012) Long-term polarization of microglia upon α-synuclein overexpression in nonhuman primates. Neuroscience 208: 85-96 Doi 10.1016/j.neuroscience.2012.02.004

5 Bian Z, Gong Y, Huang T, Lee CZW, Bian L, Bai Z, Shi H, Zeng Y, Liu C, He Jet al (2020) Deciphering human macrophage development at single-cell resolution. Nature 582: 571-576 Doi 10.1038/s41586-020-2316-7

6 Buechler C, Ritter M, Orso E, Langmann T, Klucken J, Schmitz G (2000) Regulation of scavenger receptor CD163 expression in human monocytes and macrophages by pro- and antiinflammatory stimuli. J Leukoc Biol 67: 97-103

7 Carlisle SM, Qin H, Hendrickson RC, Muwanguzi JE, Lefkowitz EJ, Kennedy RE, Yan Z, Yacoubian TA, Benveniste EN, West ABet al (2021) Sex-based differences in the activation of peripheral blood monocytes in early Parkinson disease. NPJ Parkinsons Dis 7: 36 Doi 10.1038/s41531-021-00180-z

8 Cebrian C, Zucca FA, Mauri P, Steinbeck JA, Studer L, Scherzer CR, Kanter E, Budhu S, Mandelbaum J, Vonsattel JPet al (2014) MHC-I expression renders catecholaminergic neurons susceptible to T-cell-mediated degeneration. Nature communications 5: 3633 Doi 10.1038/ncomms4633

9 Chen Y, Colonna M (2021) Microglia in Alzheimer's disease at single-cell level. Are there common patterns in humans and mice? J Exp Med 218: Doi 10.1084/jem.20202717

10 Choi I, Zhang Y, Seegobin SP, Pruvost M, Wang Q, Purtell K, Zhang B, Yue Z (2020) Microglia clear neuron-released α-synuclein via selective autophagy and prevent neurodegeneration. Nature Communications 11: 1386 Doi 10.1038/s41467-020-15119-w

11 Columba-Cabezas S, Serafini B, Ambrosini E, Sanchez M, Penna G, Adorini L, Aloisi F (2002) Induction of macrophage-derived chemokine/CCL22 expression in experimental autoimmune encephalomyelitis and cultured microglia: implications for disease regulation. J Neuroimmunol 130: 10-21 Doi 10.1016/s0165-5728(02)00170-4

12 Croisier E, Moran LB, Dexter DT, Pearce RK, Graeber MB (2005) Microglial inflammation in the parkinsonian substantia nigra: relationship to alpha-synuclein deposition. J Neuroinflammation 2: 14

13 Duffy MF, Collier TJ, Patterson JR, Kemp CJ, Luk KC, Tansey MG, Paumier KL, Kanaan NM, Fischer DL, Polinski NKet al (2018) Lewy body-like alpha-synuclein inclusions trigger reactive microgliosis prior to nigral degeneration. J Neuroinflammation 15: 129 Doi 10.1186/s12974-018-1171-z

14 Earls RH, Menees KB, Chung J, Barber J, Gutekunst C-A, Hazim MG, Lee J-K (2019) Intrastriatal injection of preformed alpha-synuclein fibrils alters central and peripheral immune cell profiles in non-transgenic mice. Journal of neuroinflammation, City, pp 250

15 Earls RH, Menees KB, Chung J, Barber J, Gutekunst CA, Hazim MG, Lee JK (2019) Intrastriatal injection of preformed alpha-synuclein fibrils alters central and peripheral immune cell profiles in non-transgenic mice. J Neuroinflammation 16: 250 Doi 10.1186/s12974-019-1636-8

16 Elfarrash S, Jensen NM, Ferreira N, Betzer C, Thevathasan JV, Diekmann R, Adel M, Omar NM, Boraie MZ, Gad Set al (2019) Organotypic slice culture model demonstrates inter-neuronal spreading of alpha-synuclein aggregates. Acta Neuropathologica Communications 7: 213 Doi 10.1186/s40478-019-0865-5

17 Etzerodt A, Kjolby M, Nielsen MJ, Maniecki M, Svendsen P, Moestrup SK (2013) Plasma clearance of hemoglobin and haptoglobin in mice and effect of CD163 gene targeting disruption. Antioxid Redox Signal 18: 2254-2263 Doi 10.1089/ars.2012.4605

18 Farmen K, Nissen SK, Stokholm MG, Iranzo A, Østergaard K, Serradell M, Otto M, Svendsen KB, Garrido A, Vilas Det al (2021) Monocyte markers correlate with immune and neuronal brain changes in REM sleep behavior disorder. Proceedings of the National Academy of Sciences 118: e2020858118 Doi 10.1073/pnas.2020858118

19 Febbraro F, Andersen KJ, Sanchez-Guajardo V, Tentillier N, Romero-Ramos M (2013) Chronic intranasal deferoxamine ameliorates motor defects and pathology in the α-synuclein rAAV Parkinson's model. Exp Neurol 247: 45-58 Doi 10.1016/j.expneurol.2013.03.017

20 Fleming SM, Ekhator OR, Ghisays V (2013) Assessment of sensorimotor function in mouse models of Parkinson's disease. J Vis Exp: Doi 10.3791/50303

21 Franklin KB, Paxinos G (2008) The mouse brain in stereotaxic coordinates. City

22 Froula JM, Castellana-Cruz M, Anabtawi NM, Camino JD, Chen SW, Thrasher DR, Freire J, Yazdi AA, Fleming S, Dobson CMet al (2019) Defining α-synuclein species responsible for Parkinson's disease phenotypes in mice. J Biol Chem 294: 10392-10406 Doi 10.1074/jbc.RA119.007743

23 Fujiwara H, Hasegawa M, Dohmae N, Kawashima A, Masliah E, Goldberg MS, Shen J, Takio K, Iwatsubo T (2002) alpha-Synuclein is phosphorylated in synucleinopathy lesions. Nat Cell Biol 4: 160-164

24 Gordon R, Albornoz EA, Christie DC, Langley MR, Kumar V, Mantovani S, Robertson AAB, Butler MS, Rowe DB, O'Neill LAet al (2018) Inflammasome inhibition prevents alpha-synuclein pathology and dopaminergic neurodegeneration in mice. Sci Transl Med 10: Doi 10.1126/scitranslmed.aah4066

25 Guo M, Wang J, Zhao Y, Feng Y, Han S, Dong Q, Cui M, Tieu K (2020) Microglial exosomes facilitate alpha-synuclein transmission in Parkinson's disease. Brain: Doi 10.1093/brain/awaa090

26 Harms AS, Delic V, Thome AD, Bryant N, Liu Z, Chandra S, Jurkuvenaite A, West AB (2017) α-Synuclein fibrils recruit peripheral immune cells in the rat brain prior to neurodegeneration. Acta Neuropathol Commun 5: 85 Doi 10.1186/s40478-017-0494-9

27 Harms AS, Ferreira SA, Romero-Ramos M (2021) Periphery and brain, innate and adaptive immunity in Parkinson's disease. Acta Neuropathologica 141: 527-545 Doi 10.1007/s00401-021-02268-5

28 Iwaki H, Blauwendraat C, Leonard HL, Makarious MB, Kim JJ, Liu G, Maple-Grodem J, Corvol JC, Pihlstrom L, van Nimwegen Met al (2021) Differences in the Presentation and Progression of Parkinson's Disease by Sex. Mov Disord 36: 106-117 Doi 10.1002/mds.28312

29 Jordão MJC, Sankowski R, Brendecke SM, Sagar, Locatelli G, Tai YH, Tay TL, Schramm E, Armbruster S, Hagemeyer Net al (2019) Single-cell profiling identifies myeloid cell subsets with distinct fates during neuroinflammation. Science 363: Doi 10.1126/science.aat7554

30 Kempthorne L, Yoon H, Madore C, Smith S, Wszolek ZK, Rademakers R, Kim J, Butovsky O, Dickson DW (2020) Loss of homeostatic microglial phenotype in CSF1R-related Leukoencephalopathy. Acta neuropathologica communications 8: 72 Doi 10.1186/s40478-020-00947-0

31 Keren-Shaul H, Spinrad A, Weiner A, Matcovitch-Natan O, Dvir-Szternfeld R, Ulland TK, David E, Baruch K, Lara-Astaiso D, Toth Bet al (2017) A Unique Microglia Type Associated with Restricting Development of Alzheimer's Disease. Cell 169: 1276-1290.e1217 Doi 10.1016/j.cell.2017.05.018

32 Klein SL, Flanagan KL (2016) Sex differences in immune responses. Nature Reviews Immunology 16: 626-638 Doi 10.1038/nri.2016.90

33 Klionsky DJ, Abeliovich H, Agostinis P, Agrawal DK, Aliev G, Askew DS, Baba M, Baehrecke EH, Bahr BA, Ballabio Aet al (2008) Guidelines for the use and interpretation of assays for monitoring autophagy in higher eukaryotes. Autophagy 4: 151-175 Doi 10.4161/auto.5338

34 Konstantin Nissen S, Farmen K, Carstensen M, Schulte C, Goldeck D, Brockmann K, Romero-Ramos M (2022) Changes in CD163+, CD11b+, and CCR2+ peripheral monocytes relate to Parkinson's disease and cognition. Brain Behav Immun 101: 182-193 Doi 10.1016/j.bbi.2022.01.005

35 Koronyo-Hamaoui M, Sheyn J, Hayden EY, Li S, Fuchs DT, Regis GC, Lopes DHJ, Black KL, Bernstein KE, Teplow DBet al (2020) Peripherally derived angiotensin converting enzyme-enhanced macrophages alleviate Alzheimer-related disease. Brain 143: 336-358 Doi 10.1093/brain/awz364

36 Krasemann S, Madore C, Cialic R, Baufeld C, Calcagno N, El Fatimy R, Beckers L, O'Loughlin E, Xu Y, Fanek Zet al (2017) The TREM2-APOE Pathway Drives the Transcriptional Phenotype of Dysfunctional Microglia in Neurodegenerative Diseases. Immunity 47: 566-581 e569 Doi 10.1016/j.immuni.2017.08.008

37 Kristiansen M, Graversen JH, Jacobsen C, Sonne O, Hoffman HJ, Law SK, Moestrup SK (2001) Identification of the haemoglobin scavenger receptor. Nature 409: 198-201 Doi 10.1038/35051594

38 Langmead B, Salzberg SL (2012) Fast gapped-read alignment with Bowtie 2. Nature Methods 9: 357-359 Doi 10.1038/nmeth.1923

39 Lassen LB, Gregersen E, Isager AK, Betzer C, Kofoed RH, Jensen PH (2018) ELISA method to detect α-synuclein oligomers in cell and animal models. PLoS One 13: e0196056 Doi 10.1371/journal.pone.0196056

40 Leclerc JL, Lampert AS, Loyola Amador C, Schlakman B, Vasilopoulos T, Svendsen P, Moestrup SK, Doré S (2018) The absence of the CD163 receptor has distinct temporal influences on intracerebral hemorrhage outcomes. J Cereb Blood Flow Metab 38: 262-273 Doi 10.1177/0271678x17701459

41 Leitenberg D, Falahati R, Lu DD, Takeda A (2007) CD45-associated protein promotes the response of primary CD4 T cells to low-potency T-cell receptor (TCR) stimulation and facilitates CD45 association with CD3/TCR and lck. Immunology 121: 545-554 Doi 10.1111/j.1365-2567.2007.02602.x

42 Li B, Dewey CN (2011) RSEM: accurate transcript quantification from RNA-Seq data with or without a reference genome. BMC Bioinformatics 12: 323 Doi 10.1186/1471-2105-12-323

43 Love MI, Huber W, Anders S (2014) Moderated estimation of fold change and dispersion for RNA-seq data with DESeq2. Genome Biol 15: 550 Doi 10.1186/s13059-014-0550-8

44 Luk KC, Covell DJ, Kehm VM, Zhang B, Song IY, Byrne MD, Pitkin RM, Decker SC, Trojanowski JQ, Lee VM (2016) Molecular and Biological Compatibility with Host Alpha-Synuclein Influences Fibril Pathogenicity. Cell Rep 16: 3373-3387 Doi 10.1016/j.celrep.2016.08.053

45 Luk KC, Kehm V, Carroll J, Zhang B, O'Brien P, Trojanowski JQ, Lee VM (2012) Pathological α-synuclein transmission initiates Parkinson-like neurodegeneration in nontransgenic mice. Science 338: 949-953 Doi 10.1126/science.1227157

46 Mahul-Mellier A-L, Burtscher J, Maharjan N, Weerens L, Croisier M, Kuttler F, Leleu M, Knott GW, Lashuel HA (2020) The process of Lewy body formation, rather than simply α-synuclein fibrillization, is one of the major drivers of neurodegeneration. Proceedings of the National Academy of Sciences 117: 4971-4982 Doi 10.1073/pnas.1913904117

47 Márquez EJ, Chung C-h, Marches R, Rossi RJ, Nehar-Belaid D, Eroglu A, Mellert DJ, Kuchel GA, Banchereau J, Ucar D (2020) Sexual-dimorphism in human immune system aging. Nature Communications 11: 751 Doi 10.1038/s41467-020-14396-9

48 Marquez EJ, Chung CH, Marches R, Rossi RJ, Nehar-Belaid D, Eroglu A, Mellert DJ, Kuchel GA, Banchereau J, Ucar D (2020) Sexual-dimorphism in human immune system aging. Nature communications 11: 751 Doi 10.1038/s41467-020-14396-9

49 McGeer PL, Itagaki S, Boyes BE, McGeer EG (1988) Reactive microglia are positive for HLA-DR in the substantia nigra of Parkinson's and Alzheimer's disease brains. Neurology 38: 1285-1291

50 Mustafa S, Martin HL, Burkly L, Costa A, Martins ML, Schwaninger M, Teismann P (2016) The role of TWEAK/Fn14 signaling in the MPTP-model of Parkinson's disease. Neuroscience 319: 116-122 Doi 10.1016/j.neuroscience.2016.01.034

51 Nagy D, Ennis KA, Wei R, Su SC, Hinckley CA, Gu RF, Gao B, Massol RH, Ehrenfels C, Jandreski Let al (2021) Developmental synaptic regulator, TWEAK/Fn14 signaling, is a determinant of synaptic function in models of stroke and neurodegeneration. Proc Natl Acad Sci U S A 118: Doi 10.1073/pnas.2001679118

52 Nguyen AT, Wang K, Hu G, Wang X, Miao Z, Azevedo JA, Suh E, Van Deerlin VM, Choi D, Roeder Ket al (2020) APOE and TREM2 regulate amyloid-responsive microglia in Alzheimer's disease. Acta Neuropathol 140: 477-493 Doi 10.1007/s00401-020-02200-3

53 Nissen SK, Ferreira SA, Nielsen MC, Schulte C, Shrivastava K, Hennig D, Etzerodt A, Graversen JH, Berg D, Maetzler Wet al (2020) Soluble CD163 Changes Indicate Monocyte Association With Cognitive Deficits in Parkinson's Disease. Mov Disord: Doi 10.1002/mds.28424

54 Patterson JR, Duffy MF, Kemp CJ, Howe JW, Collier TJ, Stoll AC, Miller KM, Patel P, Levine N, Moore DJet al (2019) Time course and magnitude of alpha-synuclein inclusion formation and

nigrostriatal degeneration in the rat model of synucleinopathy triggered by intrastriatal alpha-synuclein preformed fibrils. Neurobiol Dis 130: 104525 Doi 10.1016/j.nbd.2019.104525

55 Paumier KL, Luk KC, Manfredsson FP, Kanaan NM, Lipton JW, Collier TJ, Steece-Collier K, Kemp CJ, Celano S, Schulz Eet al (2015) Intrastriatal injection of pre-formed mouse alpha-synuclein fibrils into rats triggers alpha-synuclein pathology and bilateral nigrostriatal degeneration. Neurobiol Dis 82: 185-199 Doi 10.1016/j.nbd.2015.06.003

56 Paumier KL, Luk KC, Manfredsson FP, Kanaan NM, Lipton JW, Collier TJ, Steece-Collier K, Kemp CJ, Celano S, Schulz Eet al (2015) Intrastriatal injection of pre-formed mouse α-synuclein fibrils into rats triggers α-synuclein pathology and bilateral nigrostriatal degeneration. Neurobiol Dis 82: 185-199 Doi 10.1016/j.nbd.2015.06.003

57 Pey P, Pearce RK, Kalaitzakis ME, Griffin WS, Gentleman SM (2014) Phenotypic profile of alternative activation marker CD163 is different in Alzheimer's and Parkinson's disease. Acta Neuropathol Commun 2: 21 Doi 10.1186/2051-5960-2-21

58 Pey P, Pearce RKB, Kalaitzakis ME, Griffin WST, Gentleman SM (2014) Phenotypic profile of alternative activation marker CD163 is different in Alzheimer’s and Parkinson’s disease. Acta Neuropathologica Communications 2: 21 Doi 10.1186/2051-5960-2-21

59 Phan JA, Stokholm K, Zareba-Paslawska J, Jakobsen S, Vang K, Gjedde A, Landau AM, Romero-Ramos M (2017) Early synaptic dysfunction induced by α-synuclein in a rat model of Parkinson's disease. Sci Rep 7: 6363 Doi 10.1038/s41598-017-06724-9

60 Poewe W, Seppi K, Tanner CM, Halliday GM, Brundin P, Volkmann J, Schrag AE, Lang AE (2017) Parkinson disease. Nat Rev Dis Primers 3: 17013 Doi 10.1038/nrdp.2017.13

61 Ryter SW (2022) Heme Oxygenase-1: An Anti-Inflammatory Effector in Cardiovascular, Lung, and Related Metabolic Disorders. Antioxidants (Basel) 11: Doi 10.3390/antiox11030555

62 Samidurai M, Tarale P, Janarthanam C, Estrada CG, Gordon R, Zenitsky G, Jin H, Anantharam V, Kanthasamy AG, Kanthasamy A (2020) Tumor Necrosis Factor-Like Weak Inducer of Apoptosis (TWEAK) Enhances Activation of STAT3/NLRC4 Inflammasome Signaling Axis through PKCdelta in Astrocytes: Implications for Parkinson's Disease. Cells 9: Doi 10.3390/cells9081831

63 Samidurai M, Tarale P, Janarthanam C, Estrada CG, Gordon R, Zenitsky G, Jin H, Anantharam V, Kanthasamy AG, Kanthasamy A (2020) Tumor Necrosis Factor-Like Weak Inducer of Apoptosis (TWEAK) Enhances Activation of STAT3/NLRC4 Inflammasome Signaling Axis through PKCδ in Astrocytes: Implications for Parkinson's Disease. Cells 9: Doi 10.3390/cells9081831

64 Sanchez-Guajardo V, Febbraro F, Kirik D, Romero-Ramos M (2010) Microglia acquire distinct activation profiles depending on the degree of alpha-synuclein neuropathology in a rAAV based model of Parkinson's disease. PLoS One 5: e8784 Doi 10.1371/journal.pone.0008784

65 Smajic S, Prada-Medina CA, Landoulsi Z, Ghelfi J, Delcambre S, Dietrich C, Jarazo J, Henck J, Balachandran S, Pachchek Set al (2022) Single-cell sequencing of human midbrain reveals glial activation and a Parkinson-specific neuronal state. Brain 145: 964-978 Doi 10.1093/brain/awab446

66 Smith WW, Margolis RL, Li X, Troncoso JC, Lee MK, Dawson VL, Dawson TM, Iwatsubo T, Ross CA (2005) Alpha-synuclein phosphorylation enhances eosinophilic cytoplasmic inclusion formation in SH-SY5Y cells. J Neurosci 25: 5544-5552

67 Süß P, Hoffmann A, Rothe T, Ouyang Z, Baum W, Staszewski O, Schett G, Prinz M, Krönke G, Glass CKet al (2020) Chronic Peripheral Inflammation Causes a Region-Specific Myeloid Response in the Central Nervous System. Cell Rep 30: 4082-4095.e4086 Doi 10.1016/j.celrep.2020.02.109

68 Svendsen P, Etzerodt A, Deleuran BW, Moestrup SK (2020) Mouse CD163 deficiency strongly enhances experimental collagen-induced arthritis. Scientific Reports 10: 12447 Doi 10.1038/s41598-020-69018-7

69 Tan EK, Chao YX, West A, Chan LL, Poewe W, Jankovic J (2020) Parkinson disease and the immune system - associations, mechanisms and therapeutics. Nat Rev Neurol 16: 303-318 Doi 10.1038/s41582-020-0344-4

70 Tansey MG, Romero-Ramos M (2019) Immune system responses in Parkinson's disease: Early and dynamic. Eur J Neurosci 49: 364-383 Doi 10.1111/ejn.14290

71 Taylor JM, Brody KM, Lockhart PJ (2012) Parkin co-regulated gene is involved in aggresome formation and autophagy in response to proteasomal impairment. Exp Cell Res 318: 2059-2070 Doi 10.1016/j.yexcr.2012.05.011

72 Taylor JM, Song YJ, Huang Y, Farrer MJ, Delatycki MB, Halliday GM, Lockhart PJ (2007) Parkin Co-Regulated Gene (PACRG) is regulated by the ubiquitin-proteasomal system and is present in the pathological features of Parkinsonian diseases. Neurobiol Dis 27: 238-247 Doi 10.1016/j.nbd.2007.04.014

73 Tentillier N, Etzerodt A, Olesen MN, Rizalar FS, Jacobsen J, Bender D, Moestrup SK, Romero-Ramos M (2016) Anti-Inflammatory Modulation of Microglia via CD163-Targeted Glucocorticoids Protects Dopaminergic Neurons in the 6-OHDA Parkinson's Disease Model. J Neurosci 36: 9375-9390 Doi 10.1523/JNEUROSCI.1636-16.2016

74 Thomsen MB, Ferreira SA, Schacht AC, Jacobsen J, Simonsen M, Betzer C, Jensen PH, Brooks DJ, Landau AM, Romero-Ramos M (2020) PET imaging reveals early and progressive dopaminergic deficits after intra-striatal injection of preformed alpha-synuclein fibrils in rats. Neurobiol Dis 149: 105229 Doi 10.1016/j.nbd.2020.105229

75 Tyson T, Steiner JA, Brundin P (2016) Sorting out release, uptake and processing of alpha-synuclein during prion-like spread of pathology. J Neurochem 139 Suppl 1: 275-289 Doi 10.1111/jnc.13449

76 Van Den Eeden SK, Tanner CM, Bernstein AL, Fross RD, Leimpeter A, Bloch DA, Nelson LM (2003) Incidence of Parkinson's disease: variation by age, gender, and race/ethnicity. Am J Epidemiol 157: 1015-1022 Doi 10.1093/aje/kwg068

77 Vig M, Kinet J-P (2009) Calcium signaling in immune cells. Nature Immunology 10: 21-27 Doi 10.1038/ni.f.220

78 Villa A, Gelosa P, Castiglioni L, Cimino M, Rizzi N, Pepe G, Lolli F, Marcello E, Sironi L, Vegeto Eet al (2018) Sex-Specific Features of Microglia from Adult Mice. Cell Rep 23: 3501-3511 Doi 10.1016/j.celrep.2018.05.048

79 Volpicelli-Daley LA, Luk KC, Patel TP, Tanik SA, Riddle DM, Stieber A, Meaney DF, Trojanowski JQ, Lee VM (2011) Exogenous α-synuclein fibrils induce Lewy body pathology leading to synaptic dysfunction and neuron death. Neuron 72: 57-71 Doi 10.1016/j.neuron.2011.08.033

80 Watson MB, Richter F, Lee SK, Gabby L, Wu J, Masliah E, Effros RB, Chesselet MF (2012) Regionally-specific microglial activation in young mice over-expressing human wildtype alpha-synuclein. Exp Neurol 237: 318-334 Doi 10.1016/j.expneurol.2012.06.025

81 Wendeln AC, Degenhardt K, Kaurani L, Gertig M, Ulas T, Jain G, Wagner J, Häsler LM, Wild K, Skodras Aet al (2018) Innate immune memory in the brain shapes neurological disease hallmarks. Nature 556: 332-338 Doi 10.1038/s41586-018-0023-4

82 West MJ, Slomianka L, Gundersen HJ (1991) Unbiased stereological estimation of the total number of neurons in thesubdivisions of the rat hippocampus using the optical fractionator. Anat Rec 231: 482-497 Doi 10.1002/ar.1092310411

83 Williams GP, Schonhoff AM, Jurkuvenaite A, Thome AD, Standaert DG, Harms AS (2018) Targeting of the class II transactivator attenuates inflammation and neurodegeneration in an alpha-synuclein model of Parkinson's disease. J Neuroinflammation 15: 244 Doi 10.1186/s12974-018-1286-2

84 Wohleb ES, Franklin T, Iwata M, Duman RS (2016) Integrating neuroimmune systems in the neurobiology of depression. Nature Reviews Neuroscience 17: 497-511 Doi 10.1038/nrn.2016.69

85 Yu G, Wang LG, Han Y, He QY (2012) clusterProfiler: an R package for comparing biological themes among gene clusters. Omics 16: 284-287 Doi 10.1089/omi.2011.0118

FIGURE LEGENDS

Fig. 1 Assessment of motor performance on the Challenging Beam and the Cylinder tests. Top: Line with average and bar graphs with average and individual points show number of errors per frame, number of errors and errors/step in Frame 4 and total number of errors (summatory of Frames 2-4,) in the Challenging Beam test, 1-month post-α-syn MONO/PFF unilateral injection in the Striatum of **a-c)** males and **d-f)** females. **g-h)** Show error differences between males and females in WT and CD163KO animals. **i)** Illustration representing the portrayal of an error during a forward movement (image created with BioRender.com). **Bottom:** Bar graphs with/without individual points represent the contralateral hindlimb use (as percentage of total hindlimbs) and the number of hindlimb steps in the cylinder in **j-m)** males and **n-q)** females. Values are Mean±SEM (n=14-17 for behavior at 1-month; n=8-10 for behavior at 6-months). Statistics: Two-way ANOVA followed by Sidak's multiple comparison test. *p<0.05, **<0.01, ***<0.001

Fig. 2 Aggregated and phosphorylated α-syn expression in the striatum and interconnected regions after α-syn PFF injection. a) Representative images of MJF14 (left columns) and pSer129 α-syn immunostaining (right columns) in α-syn PFF animals 6-months p.i. Bar graphs in the bottom show average and individual points show percentage of area covered by MJF14+ staining at 1 and 6-months post-α-syn-PFF injection (respectively) in the **b,e)** Piriform Cortex and **c,f)** Amygdala, and **d,g)** the total number of cells per section in the SN at 1 and 6 months (respectively); Scale: 50μm applies to all. Values are Mean±SEM (n=6-10). Statistics: Two-way ANOVA followed by Sidak's multiple comparison test. *p<0.05, **<0.01.

Fig. 3 Differential expression of p62/SQSTM1 autophagy marker in the Substantia Nigra and Piriform Cortex after α-syn PFF injection. Box & whiskers graphs with individual points illustrate the total number of p62+ cells in the SN at **a)** 1- and **d)** 6- months p.i.. **b)** Representative images of p62/SQSTM1 immunostaining in α-syn PFF animals at **b)** 1- and **e)** 6 months p.i. in the SN and **g)** piriform cortex. **h)** Bar graphs with individual points illustrate the percentage of area covered by p62+ staining after α-syn PFF-injection in WT/CD163KO males and females. The number of p62+ cells correlated to MJF14+ cells in the SN at **c)** 1- and **f)** 6- months p.i.; the percentage of area covered by p62 + staining correlated to the one covered by MJF14+ staining **i)** in the piriform cortex at 6-months p.i. in all α-syn PFF animals. In the correlation plots: light grey symbols represent females and dark grey males. Scale bar represents 100μm in **b, e)** and 50 μm in **g)**. Values are Mean±SEM (n=6-10). Statistics: Spearman two-tail p-values (*<0.05, **<0.01), Spearman r and best-fit slope with 95% confidence intervals are plotted. Two-way ANOVA followed by Sidak's multiple comparison test. *p<0.05, **<0.01.

Fig. 4 Aggregated α-syn is associated with p62 accumulation. Representative confocal images of MJF14 (magenta) and p62 (green) and merged photo (with nuclear DAPI (Blue)) in the ipsilateral Striatum, Amygdala and Piriform Cortex of α-syn PFF animals 6 months p.i.. Squares with white dashed lines delineate the cropped region of the amplified images (upper right corner). Scale: 50 μm.

Fig. 5 CD163KO females display dysfunctional microglial and astrocytic responses to α-syn PFF injection a) Representative images of CD68 and **b)** GFAP immunostaining in α-syn PFF animals at 1 month p.i. Scale: 50μm applies to all in a-b). Bar graphs with individual points illustrate the percentage of area covered by **c,f)** CD68+ and **d,g)** GFAP+ staining after α-syn MONO and PFF injection in the striatum and **e,h)** GFAP staining after α-syn MONO and PFF injection in the SN at 1- and 6- months p.i.. **i)** Time comparison of CD68 staining in striatum between α-syn PFF groups. **j)** Representative ipsilateral images of Iba-1 immunostaining in α-syn PFF-injected animals 6 months p.i. Scale: 50μm applies to all in j). **k-m)** Bar graphs with individual points of the number of Iba-1 positive cells per mm^2 in the contralateral and ipsilateral SN, 6 months after α-syn MONO and PFF-injection. Values are Mean±SEM (n=5-10). Statistics: Two-way ANOVA followed by Sidak's multiple comparison test (*p<0.05, **<0.01, ***<0.001, ****<0.0001), or **m)** with Bonferroni corrections applied (i.e. *p<0.0125).

Fig. 6 Expression of MHCII in the Striatum and interconnected brain regions after α-syn PFF injection. a) Representative images of MHCII immunostaining in α-syn PFF animals 1 month p.i. Areas marked by gray squares in the atlas sections above represent areas photographed. Bar graphs illustrate the number of MHCII+ cells in the SN at **b)** 1- and **d)** 6 months p.i.. **c)** Box plot with individual points illustrating the scores attributed to MHCII intensity of staining in the striatum at 1 month p.i. **e)** Bar graph with individual points show the number of MHCII+ cells in the striatum at 6 months p.i. Scale:50μm applies to all. Values are Mean±SEM (n=6-10). Statistics:c) Kruskal-Wallis test; b, d-e) Two-way ANOVA followed by Sidak's multiple comparison test. *p<0.05, **p<0.01. Non-parametric test was used for c.

Fig. 7 CD4-T and CD8-T cell infiltration in the Striatum after α-syn PFF injection

a) Representative images of CD4 and CD8 immunostaining in α-syn PFF animals at 1 month p.i. Scale bars represent 50μm and 25μm for cropped images. Bar graphs with individual points of the total number of **b,d)** CD4+ and **c,e)** CD8+ cells after α-syn MONO and PFF injection in the contra- and ipsilateral striatum 1 and 6 months p.i., respectively. Values are Mean±SEM (n=6-10). Statistics: Two-way ANOVA followed by Sidak's multiple comparison test. Contralateral vs. Ipsilateral: Three-way ANOVA with matched values followed by Sidak's multiple comparisons test. # different to contralateral; ¤ different to CD163KO Female. (*p<0.05, **<0.01, ***<0.001, ****<0.0001).

Fig. 8 Striatal axonal density and stereological quantification of TH+ cell bodies in the Substantia Nigra.
a-f) Bar graphs illustrate the semi-quantitative measurement of TH+ axonal fiber density expressed as the percentage of the contralateral striatal side, post-α-syn MONO and PFF injection in the striatum. Average values of the 6 rostro-caudal striatal levels quantified are shown in **a)** Males and **b)** Females at 1 month p.i. Average and separate values of the 6 rostro-caudal striatal levels quantified are shown in **c-d)** for Males and **e-f)** Females at 6 months p.i, together with representative photos of one section at striatal level 0.38 from bregma in each group. **j)** Low magnification photos show representative nigral sections immunostained for TH and higher magnification photos show the ipsilateral SN from WT and CD163KO Male and Female mice after α-syn PFF injection. **g-n)** Stereological quantification of TH+ neurons in SN (as a percentage of contralateral). Bar graphs with individual points illustrate the average number of surviving TH+ neurons in α-syn MONO and PFF-injected WT and CD163KO males and females at **g-h)** 1- and **i,k)** 6- months p.i; **l)** Correlation between the striatal TH+ axonal density and the number of TH+ SN neurons (light grey symbols represent female and dark grey males). **m)** Quantification of TH+ neurons in WT animals (Males *vs* Females) and in **n)** CD163KO animals (Males *vs* Females). Scale bar for lower magnification photos represent 12,5mm, and in higher magnification photos 100μm as shown in **j)**. Values are Mean±SEM (n=6-10). Statistics: Two-way ANOVA followed by Sidak's multiple comparison test. *p<0.05, **<0.01, ***<0.001.

Fig. 9 Differentially expressed genes (DEGs) in Female α-syn PFF Macrophage and Microglia populations (vs. MONO). a) Bar graph showing the number of up/downregulated genes in α-syn PFF vs. MONO in Macrophage and Microglia populations 2 months p.i. **b)** Venn diagrams of shared DEGs. **c-f)** Volcano scatter-plots (-log10(padj) *vs* log2FoldChange) of DEGs in the Macrophage population and Microglia population. **g)** Gene Ontology (GO) analysis on the downregulated genes in CD163KO female macrophages. Statistics: abs (logFC)>1, FDR<0.05.

Fig. 10 Microglial *Ptprcap* upregulation in CD163KO Females and transcriptomic sex-differences. a) Volcano scatter-plots (-log10(padj) *vs* log2FoldChange) of DEGs (CD163KO vs. WT) in Females-PFF Macrophages and **b)** Microglia. **c)** STRING protein-protein interaction network with focus on *Ptprcap* gene. **d)** Bar graph showing the number of up/downregulated genes in WT Males vs. Females (α-syn PFF groups) in Macrophage and Microglia populations 2 months p.i. **e)** Gene Ontology (GO) analysis on the downregulated genes in WT-PFF (Males vs.

Females) macrophages. **f)** Volcano scatter-plot (-log10(padj) *vs* log2FoldChange) of DEGs (Males vs. Females) in CD163KO-PFF Microglia.

FIGURES

Fig. 1 Assessment of motor performance on the Challenging Beam test and Spontaneous activity on the Cylinder

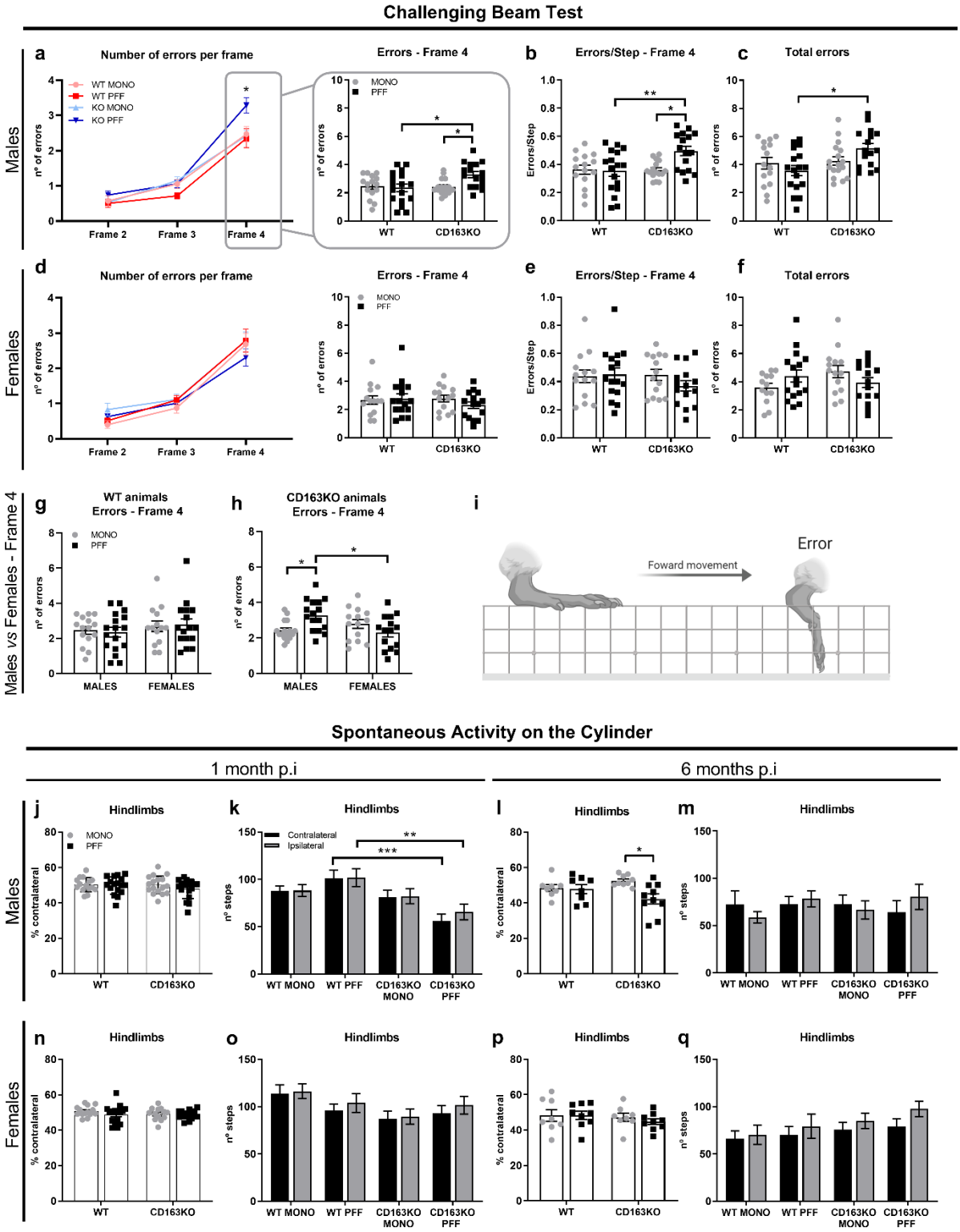

5 **Fig. 2 Aggregated and phosphorylated α-syn expression in the basal ganglia and interconnected regions to the**
6 **injection site after α-syn PFF injection.**

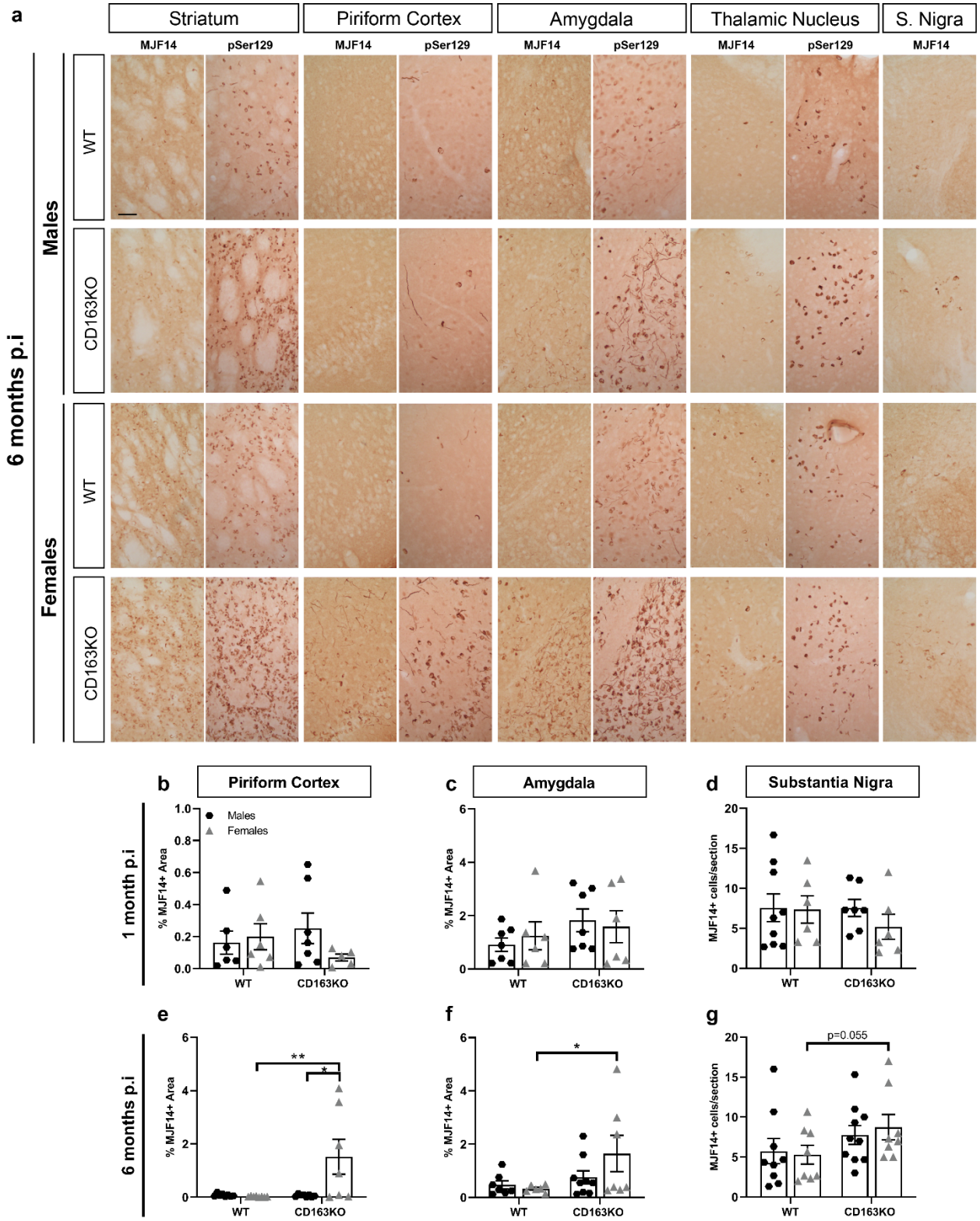

7

8 **Fig. 3 Differential expression of p62/SQSTM1 autophagy marker in the Substantia Nigra and Piriform Cortex**
9 **after α-syn PFF injection**

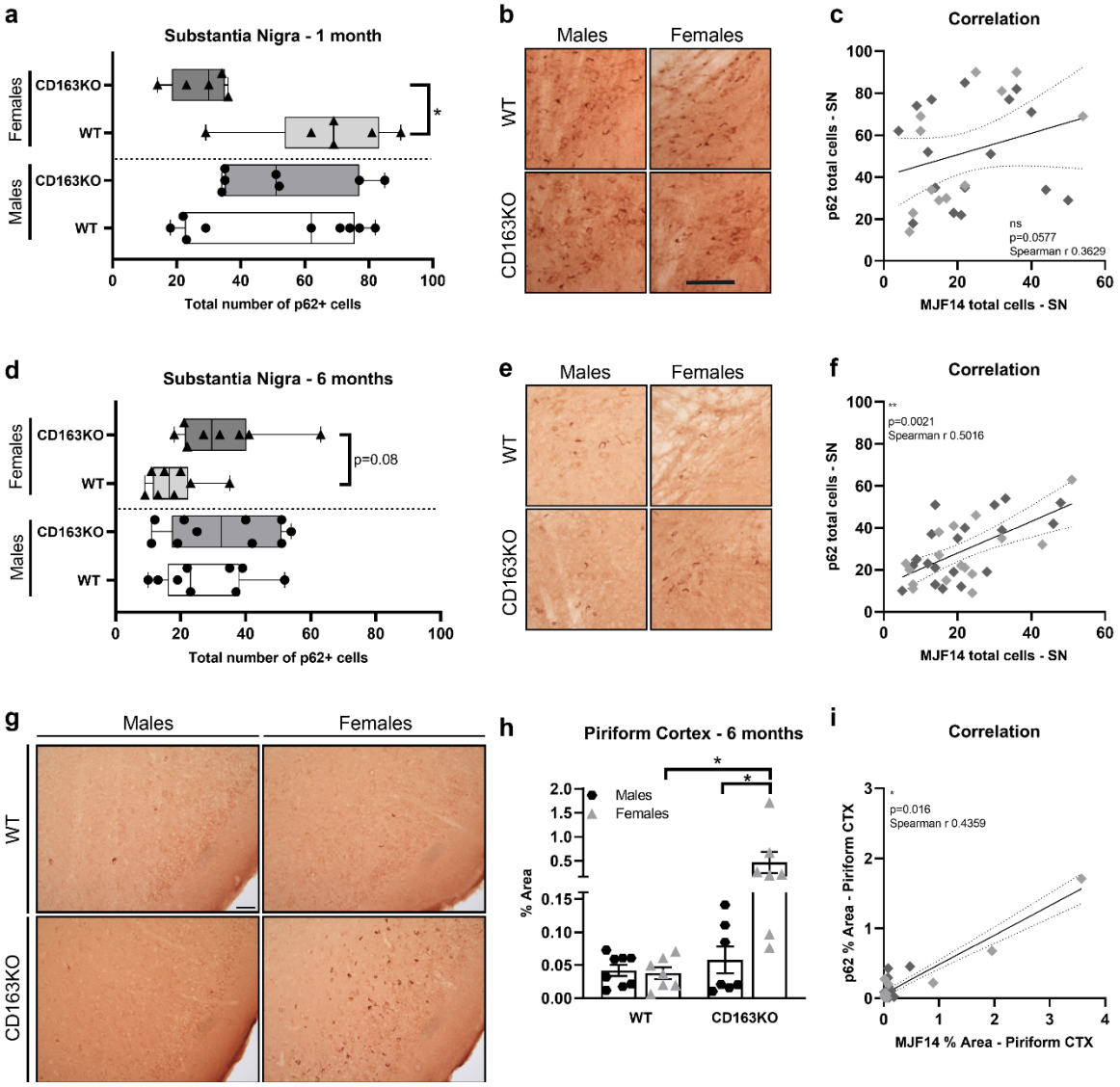

10
11
12

13

14 **Fig. 4 The progressive increase in aggregated α-syn is associated with p62 accumulation in different**
15 **interconnected brain regions.**

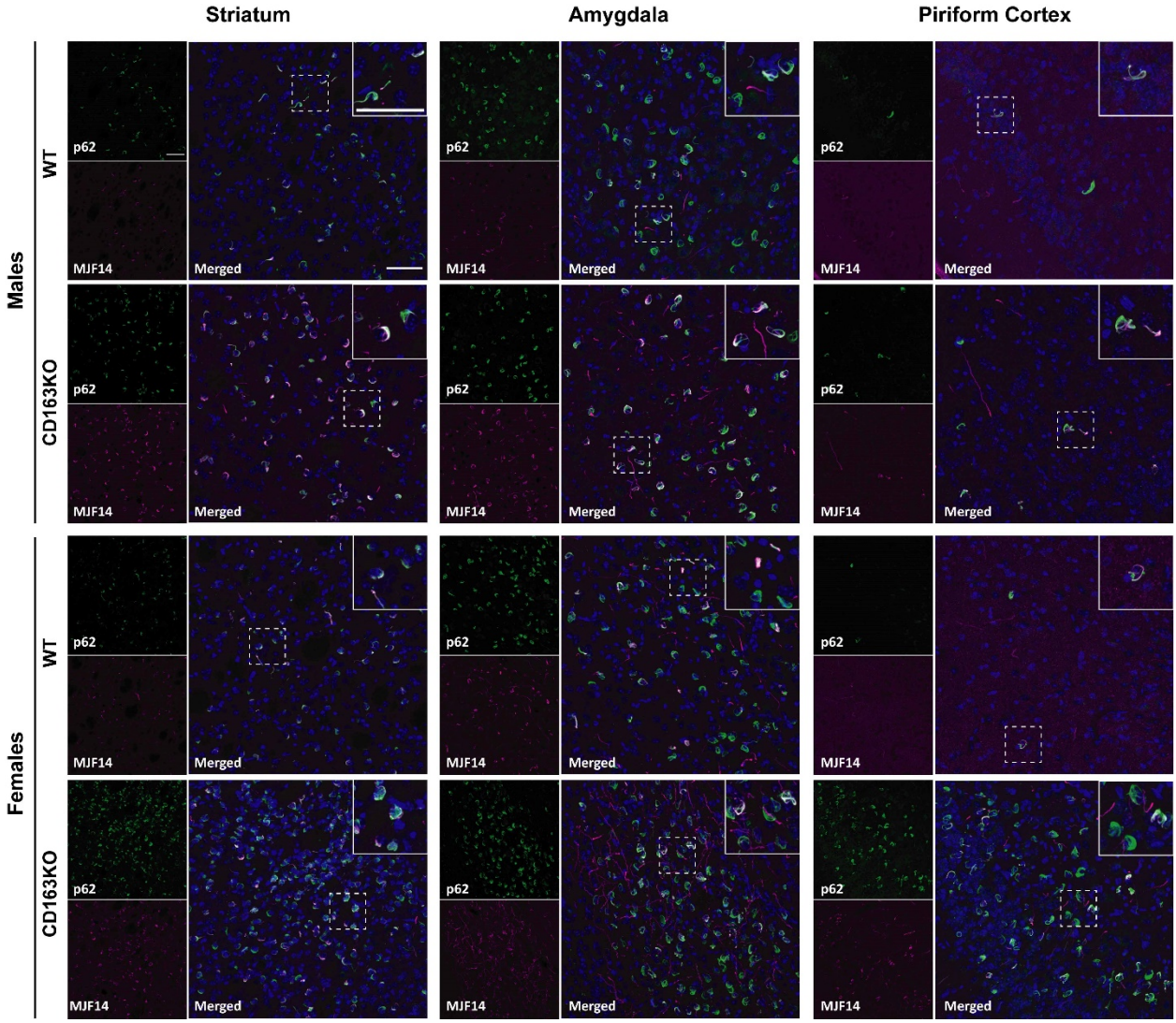

16
17
18

19 **Fig. 5 CD163KO females display dysfunctional microglial and astrocytic responses to α-syn PFF injection**

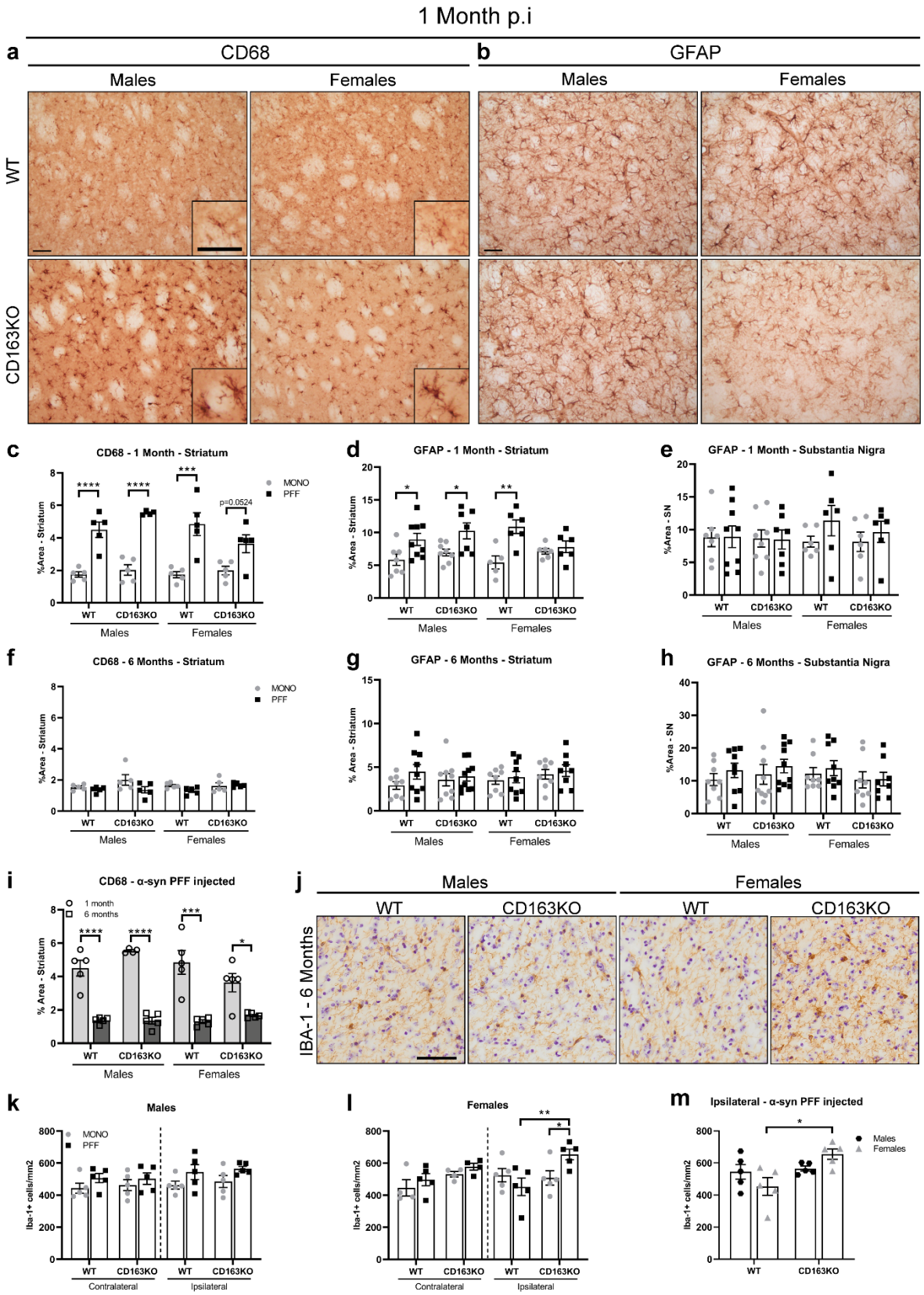

20

Fig. 6 Differential expression of MHCII in the Striatum, Substantia Nigra and interconnected brain regions after α-syn PFF injection.

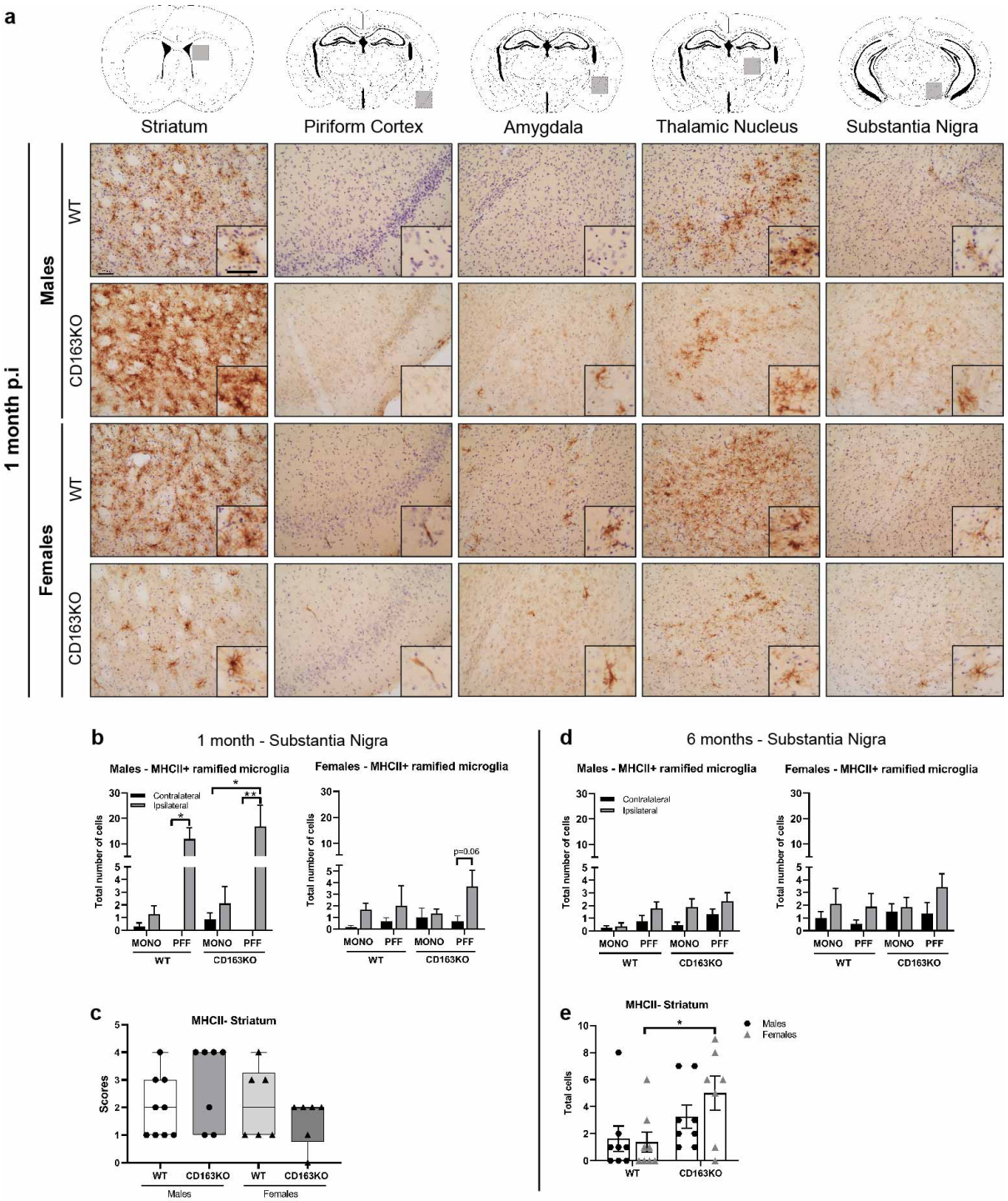

Fig. 7 CD4-T and CD8-T cell infiltration in the Striatum after α-syn PFF injection

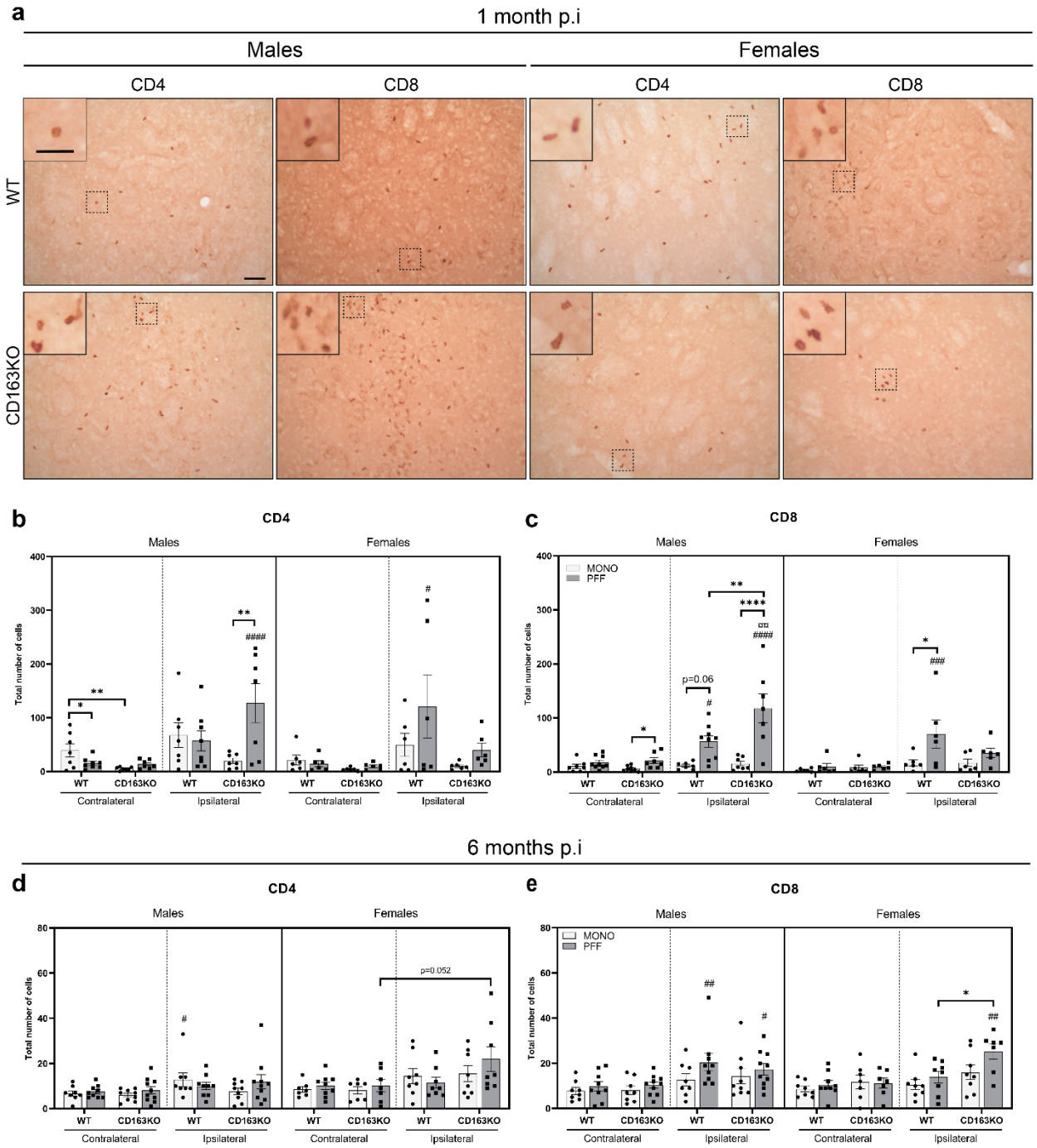

Fig. 8 Striatal axonal density and stereological quantification of TH+ cell bodies in the Substantia Nigra.

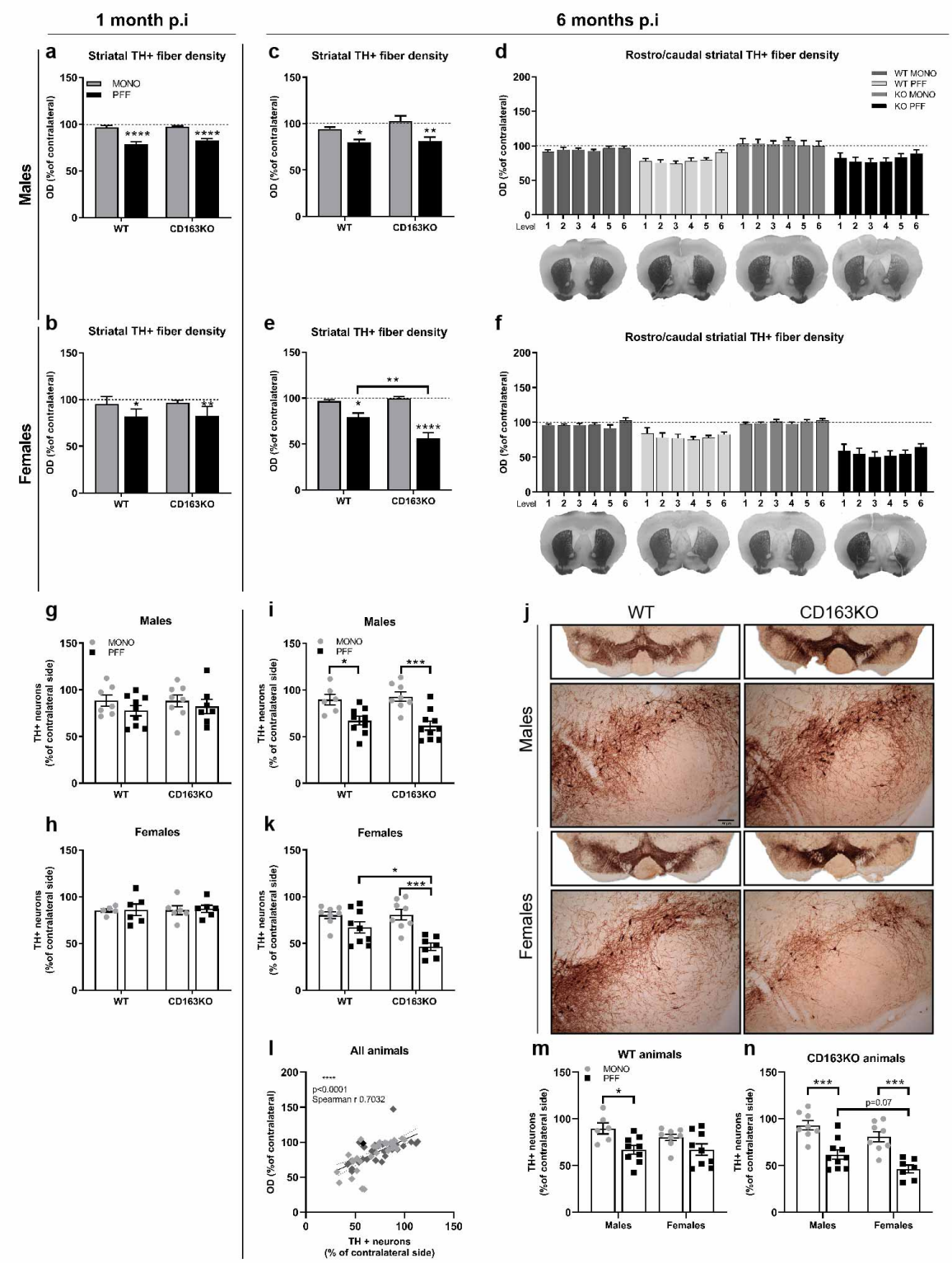

Fig. 9 Differentially expressed genes (DEGs) in Female α-syn PFF Macrophage and Microglia populations (vs. MONO).

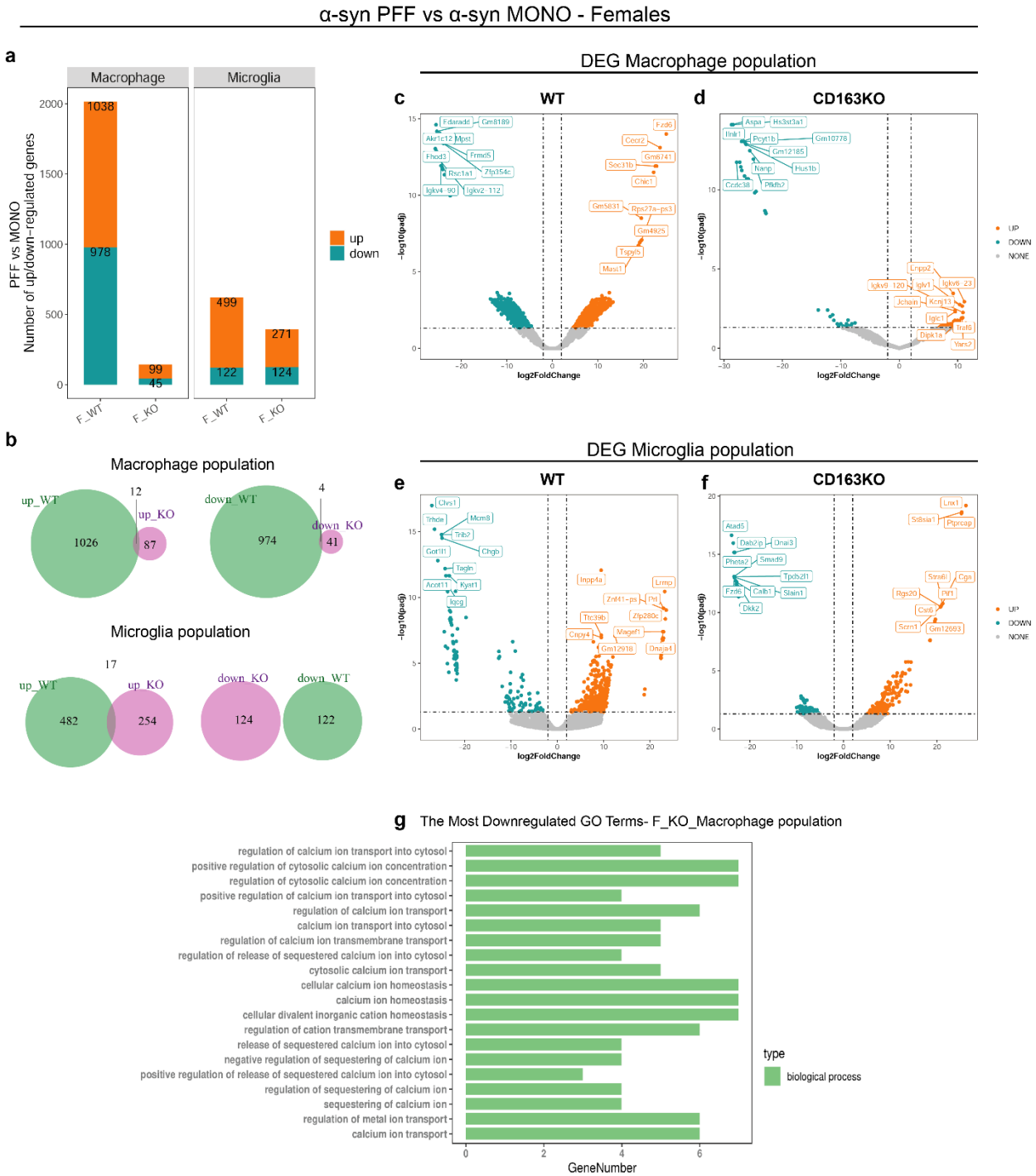
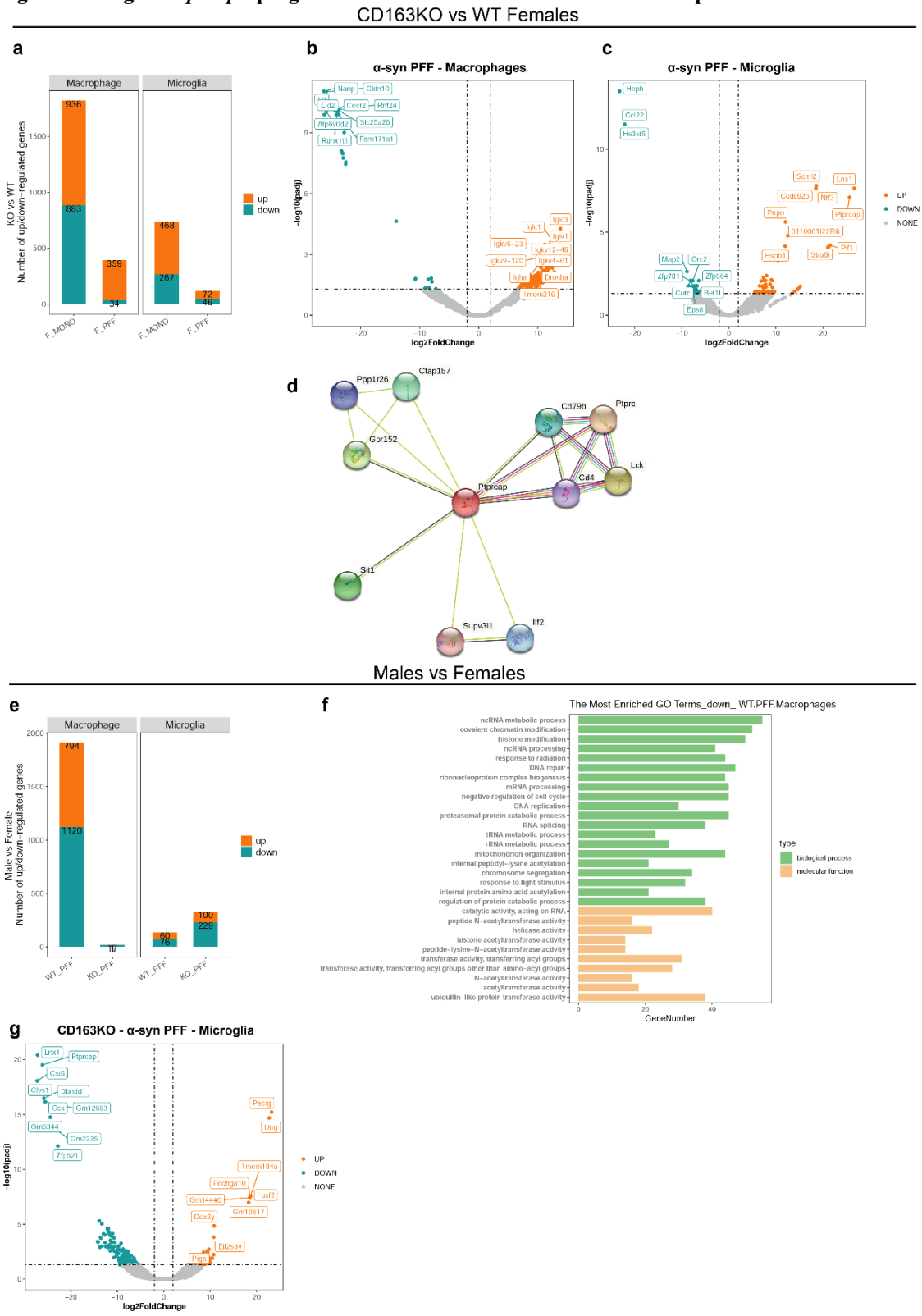
Fig. 10 Microglial *Ptprcap* upregulation in CD163KO Females and transcriptomic sex-differences.